Journal Pre-proof

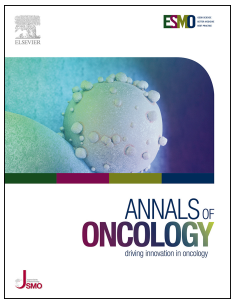

Identification, validation and biological characterization of novel Glioblastoma Tumour Microenvironment subtypes: Implications for precision immunotherapy

K. White, K. Connor, M. Meylan, A. Bougoüin, M. Salvucci, F. Bielle, A.C. O'Farrell, K. Sweeney, L. Weng, G. Bergers, P. Dicker, D.M. Ashley, E.S. Lipp, J.T. Low, J. Zhao, P. Wen, R. Prins, M. Verreault, A. Idbaih, A. Biswas, J.H.M. Prehn, D. Lambrechts, I. Arijs, F. Lodi, G. Dilcan, M. Lamfers, S. Leenstra, F. Fabro, I. Ntafoulis, J.M. Kros, J.Cryan, F. Brett, E. Quissac, A. Beausang, S. MacNally, P. O'Halloran, J. Clerkin, O. Bacon, A. Kremer, R. Tching Chi Yen, F.S. Varn, R.G.W. Verhaak, C. Sautès-Fridman, W.H. Fridman, A.T. Byrne

PII: S0923-7534(22)04743-3

DOI: https://doi.org/10.1016/j.annonc.2022.11.008

Reference: ANNONC 1148

To appear in: *Annals of Oncology*

Received Date: 5 May 2022

Revised Date: 14 November 2022

Accepted Date: 15 November 2022

Please cite this article as: White K, Connor K, Meylan M, Bougoüin A, Salvucci M, Bielle F, O'Farrell AC, Sweeney K, Weng L, Bergers G, Dicker P, Ashley DM, Lipp ES, Low JT, Zhao J, Wen P, Prins R, Verreault M, Idbaih A, Biswas A, Prehn JHM, Lambrechts D, Arijs I, Lodi F, Dilcan G, Lamfers M, Leenstra S, Fabro F, Ntafoulis I, Kros JM, J.Cryan Brett F, Quissac E, Beausang A, MacNally S, O'Halloran P, Clerkin J, Bacon O, Kremer A, Tching Chi Yen R, Varn FS, Verhaak RGW, Sautès-Fridman C, Fridman WH, Byrne AT, Identification, validation and biological characterization of novel Glioblastoma Tumour Microenvironment subtypes: Implications for precision immunotherapy, *Annals of Oncology* (2022), doi: https://doi.org/10.1016/j.annonc.2022.11.008.

during the production process, errors may be discovered which could affect the content, and all legal disclaimers that apply to the journal pertain.

Identification, validation and biological characterization of novel Glioblastoma Tumour Microenvironment subtypes: Implications for precision immunotherapy

K. White[1*,‡], K. Connor[1*,‡], M. Meylan[2], A. Bougoüin[2], M. Salvucci[1,‡], F. Bielle[3,‡], A.C. O'Farrell[1,‡], K. Sweeney[4], L. Weng[5,‡], G. Bergers[5,‡], P. Dicker[6], D.M Ashley[7], E.S. Lipp[7], J.T. Low[7], J. Zhao[8], P. Wen[9], R. Prins[10], M. Verreault[3,‡], A. Idbaih[11,‡], A. Biswas[1,‡], J.H. M. Prehn[1,‡], , D. Lambrechts[12,‡], I. Arijs[12,‡], F. Lodi[12,‡], G. Dilcan[12,‡], M. Lamfers[13,‡], S. Leenstra[13,‡], F. Fabro[13,‡], I. Ntafoulis[13,‡], J.M. Kros[14,], J.Cryan[15], F. Brett[15], E. Quissac[3], A. Beausang[15], S. MacNally[16], P. O'Halloran[16], J. Clerkin[16], O. Bacon[15], A. Kremer[17,‡], R. Tching Chi Yen[17,‡], F.S. Varn[18], R.G.W. Verhaak[18,19] C. Sautès-Fridman[2,‡], W.H. Fridman[2,‡], [#]A.T. Byrne[1,‡‡]

[1]Department of Physiology and Medical Physics, Royal College of Surgeons in Ireland, Dublin 2, Ireland;

[2]Centre de Recherche des Cordeliers, INSERM, Sorbonne Université, USPC, Université de Paris, Paris, 75006 France

[3]Paris Brain Institute (ICM), CNRS UMR 7225, Inserm U 1127, UPMC-P6 UMR S 1127, Hôpital de la Pitié - Salpêtrière - 47, boulevard de l'Hôpital –75013 Paris

[4]National Centre of Neurosurgery, Beaumont Hospital, Dublin, Ireland

[5]VIB-KU Leuven Center for Cancer Biology, Department of Oncology, KU Leuven, 3000 Leuven, Belgium

[6]Epidemiology & Public Health, Royal College of Surgeons in Ireland, Dublin, Ireland

[7]Duke Cancer Institute, Duke University, Durham, North Carolina, USA

[8]Department of Systems Biology at Columbia University, New York, NY, 10032, USA

[9]Center for Neuro-Oncology, Dana-Farber Cancer Institute, Boston, Massachusetts, USA.

[10]Department of Medical and Molecular Pharmacology, David Geffen School of Medicine, University of California, Los Angeles, Los Angeles, CA, USA

[11]Sorbonne Université, Inserm, CNRS, UMR S 1127, Paris Brain Institute (ICM), AP-HP, Hôpitaux Universitaires La Pitié Salpêtrière - Charles Foix, Service de Neurologie 2-Mazarin, F-75013, Paris, France

[12]Laboratory for Translational Genetics, Department of Human Genetics, KU Leuven, Leuven, Belgium. VIB Center for Cancer Biology, Leuven, Belgium

[13]Department of Neurosurgery, Brain Tumor Center, Erasmus University Medical Center, 3015 CN Rotterdam, The Netherlands

[14]Department of Pathology, Erasmus Medical Center, Rotterdam, Netherlands.

[15]Department of Neuropathology, Beaumont hospital, Dublin, Ireland

[16]National Centre of Neurosurgery, Beaumont hospital, Dublin, Ireland

[17]Information Technology for Translational Medicine (ITTM), Luxembourg

[18]The Jackson Laboratory for Genomic Medicine, Farmington, CT 06032, USA.

[19]Department of Neurosurgery, Cancer Center Amsterdam, Amsterdam University Medical Centers, VU University Medical Center, Amsterdam, The Netherlands

‡ Member of the GLIOTRAIN consortium

* Equal Contribution

Corresponding author: Professor Annette T. Byrne; Dept. Physiology and Medical Physics, Royal College of Surgeons in Ireland, 123 St Stephens Green, Dublin 2, Ireland; 01-402-8673; annettebyrne@rcsi.ie

Keywords: *IDH*-wt Glioblastoma; Tumour Microenvironment; Subtypes; Immunotherapy; Precision therapy

Running Title: TME subtypes may predict immunotherapy response in glioblastoma patients.

Highlights:

1. Studying the *IDH*-wt GBM tumour microenvironment (TME) transcriptome reveals three distinct GBM subtypes; TME^{High},TME^{Med}, TME^{Low}.
2. Novel TME subtypes are dynamic and evolve across primary and recurrent GBMs.
3. Interrogation of retrospective trial datasets suggest that patient response to immunotherapies could be TME subtype specific
4. $TME^{High, Med, Low}$ GBMs manifest specific contexts of vulnerability which could direct novel combinatorial treatment strategies.
5. In the future, patient assignment to TME subtypes may support precision immunotherapy treatment in IDH-wt GBM.

Abstract

Background: New precision medicine therapies are urgently required for glioblastoma (GBM). However, to date, efforts to subtype patients based on molecular profiles, have

failed to direct treatment strategies. We hypothesized that interrogation of the GBM tumor microenvironment (TME) and identification of novel TME specific subtypes could inform new precision immunotherapy treatment strategies.

Methods: A refined and validated microenvironment cell population (MCP)-counter method was applied to >800 GBM patient tumours (GBM-MCP-counter). Specifically, partition arounds medoids (PAM) clustering of GBM-MCP-counter scores in the GLIOTRAIN discovery cohort identified 3 novel patient clusters, uniquely characterised by TME-composition, functional orientation markers and immune checkpoint proteins. Validation was performed in three independent GBM-RNA-seq datasets. Neo-antigen, mutational, and gene ontology analysis identified mutations and uniquely altered pathways across subtypes. The longitudinal GLASS cohort and three immunotherapy clinical trial cohorts (treatment with neoadjuvant/adjuvant anti-PD1 or PSVRIPO) were further interrogated to assess subtype alterations between primary and recurrent tumours, and to assess the utility of TME classifiers as immunotherapy biomarkers.

Results: TME^{High} tumours (30%) displayed elevated lymphocyte, myeloid cell immune checkpoint, PDCD1(PD1) and CTLA4 transcripts. TME^{High}/mesenchymal+ patients featured tertiary lymphoid structures (TLS). TME^{Med} (46%) tumours were enriched for endothelial cell gene expression profiles and displayed heterogeneous immune populations. TME^{Low} (24%) tumours were manifest as an 'immune-desert' group. TME-subtype transitions upon recurrence were identified in the longitudinal GLASS cohort. Assessment of GBM immunotherapy trial datasets revealed that TME^{High} patients receiving neo-adjuvant anti-PD1 had significantly increased OS (P=0.04). Moreover, TME^{High}

patients treated with adjuvant anti-PD1 or oncolytic virus (PVSRIPO), showed a trend towards improved survival.

Conclusions: We have established a novel TME-based classification system for application in intracranial malignancies. TME-subtypes represent canonical "*termini a quo"* (starting points) to support an improved precision immunotherapy treatment approach.

Introduction

Elucidation of IDHwt GBM[1] disease subtypes[1] based on mutational profiling, gene expression and DNA methylation has failed to translate into improved clinical outcomes[2]. GBM tumours are complex ecosystems composed of diverse malignant (e.g. stem) and non-malignant (e.g. glial, microglia, immune cells, vascular cells, reactive astrocytes) cell populations which exist in several niches, interact with heterogeneous tumour cells[3] and exhibit a dynamic heterogeneity and plasticity. Of late, there has been much focus on targeting the GBM immune cell niche, notwithstanding a generalized immunosuppressive microenvironment in the intracranial setting. For example, as the immune checkpoint protein PD-L1 is expressed in GBM[4,5] and pre-clinical data[6,7] provided rationale for evaluation of immune checkpoint inhibitors (ICIs), multiple clinical studies have now been completed. Disappointingly, these trials have been negative[8–12] most likely as limited patient stratification methods were available to rationally select patients who might benefit most from treatment. Nevertheless, a small multicentre randomised control trial

conducted in the setting of recurrent GBM (rGBM) suggests that neo-adjuvant anti-PD-1 blockade may elicit enhanced immune responses and survival benefits[13].

In the current study, the GLIOTRAIN consortium (www.gliotrain.eu), together with US collaborators, have interrogated tissue-infiltrating immune and stromal cell populations of selected GBM patients using a modified targeted microenvironment cell-population counter (MCP-counter) RNA-seq computational method[14]. Unsupervised partition around medoids (PAM) clustering identified three novel TME-associated subtypes designated TME^{low}, TME^{med}, and TME^{high} which have been validated in publicly available datasets. To provide insight into novel subtype-specific biology, we analyzed TME functional orientation markers and differentially expressed genes. Moreover, we performed mutational analysis and neoantigen prediction across novel subtypes, and have longitudinally assessed subtype switching events in primary and recurrent tumours. Finally, the capacity of novel TME-subtypes to predict outcome was assessed in retrospective immunotherapy clinical trial datasets. Our findings lay the foundation for a novel subtyping approach which may be applied, to direct novel combinatorial immunotherapy strategies in the brain tumour setting.

Materials and Methods

Patient Series (N=867 samples, N=8 cohorts)

GLIOTRAIN Discovery cohort

Informed consent for use of multi-omics data and associated clinical annotation was obtained via appropriate institutional channels. The GLIOTRAIN cohort was comprised of

123 retrospectively collected fresh frozen (FF) GBM samples, acquired at time of surgery, with corresponding clinical follow-up data. Patient samples were collected based on the GLIOTRAIN biobank inclusion criteria (Table 1). FF tumour samples from three participating institutions were collected (Table 2) and clinical data associated with GLIOTRAIN samples are described in Table 3.

Validation and Glioma Longitudinal Analysis Consortium (GLASS) Longitudinal Cohorts

Transcriptomic and clinical data from the Cancer Genome Atlas Glioblastoma Multiforme (TCGA-GBM) data collection was downloaded from the National Cancer Institute Genomic Data Commons (GDC) data portal (TCGA RNA-seq cohort)[15]. mRNAseq_693 (batch 1) dataset and clinical data was downloaded from the Chinese Glioma Atlas database (http://www.cgga.org.cn)(CGGA RNA-seq cohort)[16]. The DUKE cohort comprised GBM patients treated at Duke's Preston Robert Tisch Brain Tumor Center (RNA sequencing performed by Caris Life Sciences). The GLASS dataset (GLASS cohort) was downloaded from Synapse (https://www.synapse.org/#!Synapse:syn17038081/wiki/585622)[17].Clinical annotation for DUKE and GLASS datasets provided from collaborators upon request and described in Table 3 and 4 respectively.

Immunotherapy Trial Cohorts

Transcriptomic data for GSE121810 were provided upon request (Cloughesy cohort[13]). Transcriptomic data was downloaded from SRAPRJNA482620 (Zhao cohort[18]). RNAseq bam files for the PVSRIPO clinical trial were downloaded from Genotypes and

Phenotypes (dbGaP) database (PVSRIPO cohort). Clinical annotation for all datasets was also provided. [19] (Table 5 and 6). Discovery, validation, GLASS longitudinal and immunotherapy clinical trial cohorts were filtered as outlined (Supplementary figure 1).

For detailed descriptions of next generation sequencing methods, MCP-counter modification, interrogation of TME composition and validation of novel TME subtypes, Wang subtype classification, neoantigen prediction, multiplexed immunohistochemistry methods, IvyGAP dataset analysis, gene ontology analysis and statistical methods, see supplementary materials, at *Annals of Oncology* online.

Results

Modification and Validation of MCP-counter for application in GBM

We first established the MCP-counter method for application in GBM (GBM-MCP-counter). Specifically, we removed fibroblast scores, and a GBM-specific microglial signature described by KLEMM et al[20], was incorporated. Next we validated GBM specific gene expression at the protein level by IHC and IF (Supplementary Figure 2A). Correlations between GBM-MCP scores of immune cell populations and corresponding IHC cell density (Supplementary Figure 2B) were confirmed. CD3 T cells, CD8 T cells and monocytic lineage showed high correlation coefficients with IHC protein cell density evaluations (R= 0.43, 0.52, and 0.44, P=0.031, 0.012 and 0.048 respectively). Microglia expression signature significantly correlated with microglia IF panel cell density (CD68-/Iba1+/TMEM119) (R=0.56, P=0.0047) (Supplementary Figure 2B).

Identification of novel TME-subtypes

Partition around medoids (PAM) clustering, based on patient GBM-MCP-counter scores, was performed on the GLIOTRAIN cohort. Clustering identified 3 distinct, novel subtypes with significantly different TME compositions (silhouette statistic methods and principal component analysis (PCA) (Supplementary Figure 3A-D). These subgroups were defined as TME^{Low}, 'Immune-Low', (24%), TME^{Med}, 'heterogenous immune populations', (46%) and TME^{High}, 'Immune-High' (30%) (Figure 1A). These findings were reproduced in TCGA, CGGA and DUKE datasets (Figure 1B-D, Supplementary Figure 4, Supplementary Figure 5). A representative cohort (*N*=26), from /span>GLIOTRAIN (GLIOTRAIN-IHC cohort) was assigned to TME-subtypes (Supplementary Figure 6A) and quantitative IHC data orthogonally validated each TME-subtype (Supplementary Figure 6B,C)[14]. Overall, GBM-MCP-counter analysis revealed that TME^{High} cases are characterized by significantly increased expression of genes specific to all immune populations (Figure 1A-D). TME^{Med} cases were characterised by high endothelial cell GBM-MCP signature, and heterogenous abundance of immune cells. Notably, the microglial signature was enriched in both TME^{High} and TME^{Med} subtypes (Figure 1A). Finally, the TME^{Low} subtype was characterised by a low expression of all immune and endothelial cell markers (Figure 1A-D). Stratification into TME^{High}, TME^{Med} or TME^{Low} subtypes showed no association with OS in GLIOTRAIN, TCGA, CGGA and DUKE cohorts (*P*=0.55, *P*=0.53, *P*=0.13, and *P*=0.55 respectively)(Figure 1E-H).

We subsequently studied the association of proneural (PN), classical (CL) and mesenchymal (Mes) gene expression subtypes[21] with novel TME-subtypes identified. TME^{High} tumours comprised of 23% PN, 18% CL and 59% Mes cases. TME^{Med} were comprised of 41% PN, 26% CL and 33% Mes, and TME^{Low} 55% CL, 35% PN and 10% Mes (Figure 1I). Findings remained consistent across all validation cohorts (Figure1B-D). Survival analysis following Wang subtype patient stratification[21] (PN, CL, Mes) showed no significant impact on OS in any cohort (Supplementary Figure 7A-C).

Biological characterisation of TME-subtypes

Next, we studied TME composition and functionality across subtypes. Expression of genes associated with functional orientation markers were significantly enriched in the TME^{High} subtype (Figure 2A) in the GLIOTRAIN cohort. Angiogenesis signature expression was homogenous across all TME-subtypes (*P*=0.38)(Figure 2A). The expression of immune-checkpoint-related genes showed a similar trend to immune infiltrate genes, with high expression of genes encoding PD1 and CTLA4 observed in the TME^{High} subtype (*P*=2.1e-05, *P*=1.4e-06)(Figure 2A). *CD274* (which encodes PDL1) was significantly enriched in TME^{High} GBM and heterogeneously expressed across all TME-subtypes (*P*=0.0053), whereas *TIM3* was homogenously expressed across all subtypes (Figure 2A, Supplementary Figure 5A-C). Notably, B7 homolog 3 protein (B7-H3/CD276[22]) expression was significantly downregulated in TCGA cohort TME^{High} patients (*P*=0.012; Figure S7A). No significant difference in B7-H3 expression was observed across novel TME subgroups in other cohorts (Figure 2A, Supplementary Figure 8B, C). Interestingly, several previous

studies assessing B7-H3 expression in GBM have observed similar diverse expression patterns[23–25].

We further interrogated TME-subtype mutational landscape within the TCGA RNA-seq cohort, where matching WES data were available. As expected, tumour mutational burden (TMB) was low (median: 48 mutations)[Data not shown]. Moreover, mutational analysis revealed no difference in neo-antigen prediction or mutation count across TME-subtypes (Kruskal-Wallis, *P*=0.14 and *P*=0.081 respectively)(Figure 2B,C). Nevertheless, a small number of genes were frequently mutated in specific TME-subtypes. Specifically, *EGFR* was most frequently mutated in TME^{Low} GBM, *TTN* in TME^{Med} and *PTEN* in TME^{High} tumours (Figure 2D). Interestingly, IHC analyses (CD20+/CD3+), revealed tertiary lymphoid structures (TLS) as a possible feature of TME^{High}/$Mesenchymal^{+}$ GBM (Supplementary Figure 9A, B). Survival analysis in the GLIOTRAIN cohort based on TLS associated 12-chemokine signature[26,27] suggested monocytic lineage in TLS^{High} patients display suppressed immune responses (Supplementary figure 9C, D). Furthermore, TLS^{High} patients displayed enriched genes associated with T-cell activation and may therefore be able to elicit an immune response (Supplementary figure 9E). We also analysed MGMT promoter methylation status across novel TME subtypes in the GLIOTRAIN, TCGA, CGGA and DUKE cohorts (Supplementary Figure 10). Overall, no significant relationship was observed between MGMT status and TME subtype.

Differential gene expression analysis across TME-subtypes revealed several significantly down-regulated genes in the TME^{Low} subtype when compared to non-TME^{Low} samples

(Figure 2E). Interestingly, some of the most significantly downregulated genes (SLC2A5, CSF3R) were microglial-related. TME^{Med} was associated with several downregulated genes, including the B lymphocyte chemoattractant and TLS marker, CXCL13 compared to non-TME^{Med} samples (Figure 2F). Whereas TME^{High} GBM predominantly consisted of significantly upregulated genes including genes encoding for T-lymphocytes (CD6), surface antigens on T-cells (CD2) and cytokine CCL5 compared to non-TME^{High} samples (Figure 2G). Gene Ontology (GO) enrichment analysis in the GLITRAIN cohort revealed TME-subtype specific pathway alterations. TME^{Low} GBM was significantly enriched in pathways relating to EGFR signalling (*P*=0.02406)(Supplementary Figure 11A), and showed significantly downregulated immune-related pathways (Supplementary Figure 12A). TME^{Med} was enriched in pathways relating to neuronal signalling (Supplementary Figure 11B) and displayed downregulated immune-related pathways (Supplementary Figure 12B). TME^{High} GBM was significantly enriched in pathways relating to the immune system, including complement cascade and immunoregulatory interactions between lymphoid (*P*=2.4e-37) and non-lymphoid cells (*P*=7.9e-34)(Supplementary Figure 11C). In contrast, few significantly downregulated pathways were observed in TME^{High} (Supplementary Figure 12C).

To address spatial heterogeneity of TME subtype expression signatures, the IvyGAP dataset (*N*=122 samples) was stratified according to novel TME classifiers (Supplementary Figure 13A). Spatial interrogation of TME subtype distribution (based on IvyGAP anatomic neighbourhoods), identified differing gene expression patterns among each anatomic region. TME^{High} samples were most enriched within regions defined as

cellular tumour (63%). TME^{High} samples also demonstrated slightly elevated proportions of microvascular proliferation samples (12%) compared to other subtypes. The TME^{Med} cohort manifested a moderate proportion of infiltrating tumour samples (10%) and elevated proportion of microvascular proliferation samples (15%) compared to TME^{Low} samples (6%). In contrast, TME^{Med} samples displayed the highest proportion of pseudopalisading cells around necrosis samples (23%). Finally, the TME^{Low} cohort contained the highest proportion of infiltrating tumour (14%) and leading edge (12%) samples. An additional subgroup (12.6%), which displayed an enriched expression of endothelial (*P*=<2.2e-16) and myeloid dendritic cells (p=3.5e-16), was further identified upon IvyGAP sample clustering (Cluster EC, Supplementary Figure 13). This cluster most frequently manifested with leading edge samples (20%) compared with TME^{Low}, TME^{Med} or TME^{High} subtypes (Supplementary Figure 13B).

Longitudinal analysis of TME-subtypes reveals TME-subtype 'switch' on recurrence

To assess TME-subtype evolution and identify changes in TME composition at tumour recurrence, we next analysed a set of longitudinal transcriptomic data from the GLASS longitudinal cohort (*N*=99 patients with primary and recurrent tumours)[17]. FirstlyTME-subtypes were applied to primary and recurrent GLASS cohort tumours (*N*=367 tumour samples representing primary and recurrence 1-4), followed by assessment of functional orientation markers and immune checkpoint expression. These analyses revealed T cells, CD8 T cells, B lineage and PD1 expression were significantly enriched in recurrent tumours (Figure 3A). Next, we categorised the GLASS cohort according to novel TME-subtypes (Supplementary Figure 14A) identifying a higher proportion of TME^{Med} (39%) and

TME^{High} (22%) cases in recurrent samples when compared to primary tumours (33% and 12% respectively)(Figure 3B,C). The proportion of TME^{Low} tumour s decreased from 55% to 39% upon recurrence. Tumours which transitioned from TME^{Low} to TME^{Med} upon recurrence, presented significantly elevated lymphocyte-associated gene expression. Specifically, T cells (*P*=5.4e-06), CD8 T cells (*P*=2.3e-10), cytotoxic lymphocytes (*P*=0.022) and B lineage (*P*=0.00085) expression markers were elevated (Figure 3D). TME^{Low} to TME^{High} transitions revealed significantly enriched lymphocytes and monocytic lineage (Figure 3E). TME^{Med} to TME^{High} subtype transition showed a significant enrichment across immune and stromal cell populations (excluding microglia)(Figure 3F). Unsurprisingly, tumours which switched to more immune cold subtypes displayed significantly decreased immune populations (Supplementary Figure 14B,C). In depth cell-state analysis revealed TME^{Med} to TME^{High} transition was influenced by a significantly enriched myeloid cell state *(P*=0.0019). Moreover, Stem-like and diff-like neoplastic states were significantly downregulated upon this transition (*P*=0.04 and *P*=0.00049 respectively)(Supplementary Figure 15A-C). DEG analysis revealed several significantly upregulated chemokine-signalling related pathways upon TME^{Med} to TME^{High} switch (Supplementary Figure 15D). Moreover, tumour promoting chemokines, CCL18 and ACP5, were highly upregulated upon subtype switch (Supplementary Figure 15E). In a very limited number of available longitudinal GLASS cohort samples (*N*=4) from patients treated with immunotherapy, we assessed whether trends in TME subtype switch are altered following treatment (Supplementary Figure 14D). Unsurprisingly, findings were inconclusive, with transitions from TME^{Med} to TME^{Low} (*N*=1), TME^{Med} to TME^{High} (*N*=1) and TME^{Low} to TME^{Med} (*N*=2) observed.

TME-subtypes may inform treatment outcome in retrospective immunotherapy trial datasets

We subsequently examined whether patient stratification based on TME-subtype could predict response to immune checkpoint blockade. To this end, we accessed RNA-seq and clinical annotation data from the recent neoadjuvant anti-PD1 multi-institution clinical trial (Cloughesy cohort)[13]. This trial evaluated immune responses and survival following neoadjuvant and/or adjuvant therapy with pembrolizumab in patients with recurrent, surgically-resectable GBM. Firstly, IDHmt samples (*N*=4) were identified and excluded. Subsequently, TME classifiers were assigned to the trial cohort (Figure 4A). TME^{High} tumour-bearing patients displayed a trend towards improved OS when compared with TME^{Low} and TME^{Med} tumour-bearing patients (*P*=0.29)(Figure 4B). Importantly, TME^{High} patients treated with neoadjuvant anti-PD1 exhibited a significantly increased OS compared with neoadjuvant anti-PD1 treated non-TME^{High} (TME^{Low} and TME^{Med}) patients and TME^{Med} patients treated with adjuvant anti-PD1 (*P*=0.028)(Figure 4C,D).

Next, to further study the relationship between TME-subtype and response to ICI, we accessed RNA-seq data from the Zhao study (Zhao cohort) which evaluated immune responses and survival of longitudinally profiled patients during standard therapy and following treatment with PD-1 inhibitors (nivolumab or pembrolizumab)[18]. Firstly, the GBM-MCP-counter was applied to pre- and post-anti-PD1 treated tumour samples (n=24)(Figure 5A). Comparison of pre- and post-treatment samples revealed tumours receiving adjuvant anti-PD1 displayed no significantly different GBM-MCP scores. Next,

samples were assigned to novel TME-subtypes. Survival analysis showed a trend towards improved OS in TME^{High} compared to non-TME^{High} patients (TME^{Low}/TME^{Med})(*P*=0.21)(Figure 5B). We subsequently assessed how TME-subtype proportion changes in pre- and post-anti-PD1 treatment samples, and in responders and non-responders (responders defined as those which revealed an inflammatory response, few tumour cells upon sampling and stable or shrinking tumour volume). Following anti-PD1 treatment, the proportion of TME^{Low} tumours remained the same (33%), the proportion of TME^{Med} tumours decreased from 27% to 22%, and the proportion of TME^{High} tumours increased from 40% to 44% (Figure 5C). Based on pre-treatment tumour samples, TME^{Low} proportion was greater in responders (7%) compared to non-responders (20%). Likewise, 43% of TME^{High} were responders compared with 40% non-responders. No TME^{Med} samples were categorised as responders (Supplementary Figure 16). Comparison of GBM-MCP scores in non-responders and responders, and in pre- and post- ICI treated (*N*=3) samples (Supplementary Figure 17) indicated no significant changes in TME populations.

Finally, we examined whether patient stratification based on TME-subtype could predict response to oncolytic virus therapy. Sequencing and clinical data were accessed from the Desjardins et al [19] 2018 phase 1 clinical trial (NCT01491893) which evaluated convection-enhanced, intratumoral delivery of recombinant non-pathogenic polio–rhinovirus chimera (PVSRIPO) in rGBM patients (PVSRIPO cohort). Samples were first assigned to TME-subtypes (Figure 5E). Tentatively, TME^{High} patients treated with PVSRIPO showed a trend

towards improved OS (*P*=0.056) when compared with TME^{Low} and TME^{Med} tumours (Figure 5F).

Discussion

Notwithstanding the plausible rationale which has supported immune checkpoint inhibitor evaluation in GBM trials,[7,28] to date, clinical studies have largely been negative[9,10] with few exceptions[13,29,30]. Of these, [3132]recent data from a small multi-centre trial (Cloughesy study) suggests that neoadjuvant nivolumab may improve OS compared to patients receiving adjuvant therapy[13]. Furthermore, mechanistic interrogation of the immunemicroenvironment following administration of neo-adjuvant nivolumab revealed increased immune cell infiltration, chemokine transcript expression and greater T-cell antigen receptor (TCR) diversity among TILs[29]. Notwithstanding these important, hypothesis generating data, most negative clinical trial outcomes[9–12] now mandate the identification of new stratification methods to identify a sub-population of patients for whom immunotherapy could be a viable option. To this end, we hypothesized that interrogation of the TME, including the identification of novel TME-associated subtypes might predict which patients would be most responsive to immunotherapy and have generated robust hypotheses for novel subtype-specific combinatorial immunotherapy treatment regimens, which now warrant further testingspan style="font-family:Arial"> [2].

To identify novel TME specific classifiers, we implemented a tailored, brain tumour-specific MCP-counter[14] method. Specifically, unsupervised PAM clustering was applied to

GBM-MCP-counter scores in discovery and validation cohorts (*N*=867 primary/recurrent patient samples) to identify three, non-overlapping TME-subtypes: TME^{Low}, TME^{Med}, and TME^{High}. Survival analysis revealed that there was no subtype-specific prognostic association. This is unsurprising as discovery and validation cohorts were normalized for KPS and age and included only IDHwt samples. Moreover, GBM-MCP-counter scores are based on genes which have no clear prognostic value when assessed as individual biomarkers[31]. We observed an overlap between novel TME-subtypes and Wang transcriptomic classifiers. However we observed no survival differences following classification according to Wang-subtypes[21]. There was no significant difference in neoantigen load across TME classifiers, and a low tumour mutational burden was observed across all subtypes. Interestingly, Zhang et al have recently shown that methylated MGMT and low TIM3 expression are associated with improved survival in GBM[32]. However, in our analyses TIM3 expression was homogenous across subtypes. No significant relationship was observed between MGMT methylation status and novel TME subtype.

TME^{Low} GBM is associated with low immune and endothelial cell abundance, low expression of genes associated with TME functional orientation and overall downregulated immune-regulatory pathways TME^{Low} tumours also manifested the highest proportion of infiltrating tumour and leading-edge samples within the IvyGAP cohort compared to TME^{High} and TME^{Med} patient samples. Mutational and GO analysis showed that EGFR mutation and upregulated EGFR signaling pathways were dominant features of TME^{Low} GBM. As TME^{Low} patients exhibit overall low immune cell abundance, our data

indicate that patients categorised as TME^{Low} may be the most suitable candidates for a prospective clinical trial evaluating the combination of anti-TIM3 combined with an EGFR inhibitor. This strategy would concurrently target the high EGFR mutational burden of TME^{Low} patients whilst stimulating T-cell infiltration. Recently, it has been suggested that EGFR therapeutic resistance may arise due to extrachromosomal DNA (ecDNA) amplification, rather than classical chromosomal alterations[33]. Further interrogation of TME^{Low} ecDNA landscape is required to uncover potential resistance mechanisms which may be hallmarks of this subtype.

TME^{Med} GBM is associated with an abundance of immune populations, functional orientation markers, immune checkpoint and endothelial cell markers. TME subtype analysis of IvyGAP anatomical samples revealed TME^{Med} patients comprised the highest proportion of samples defined as 'pseudopalisading cells around necrosis'. Interestingly, pseudopalisades are associated with microvascular hyperplasia and angiogeneisis, and may serve as predictors of poor prognosis in GBM[34]. Thus, despite negative outcomes following anti-angiogenic therapy (NCT00884741 and Checkmate-143/NCT02017717), our data tentatively suggests that patients identified in the 'colder' TME^{Med} subtype might anti-angiogenic treatment combined with immunotherapy due to high endothelial cell abundance, vascularity and diverse immune cell population. Additionally, titin (TTN) mutation was identified as a TME^{Med} tumour feature. While TTN mutations are associated with favourable prognosis in non-small cell lung cancer[35], mutant TTN may be associated with increased risk of glioma recurrence[36] suggesting that TTN mutations could influence GBM TME^{Med} tumour recurrence. GO analysis of TME^{Med} tumours further revealed

upregulated neuronal system-related and transmission across chemical synapses pathways. We and others have recently shown that increased GBM growth and invasion is facilitated by neuron-to-glioma synapses and increased neuronal interactions at recurrence[37,38]. Overall, future studies are now required to interrogate the role of TTN and neuronal-tumour interactions in TME^{Med} GBM recurrence and tumour progression.

TME^{High} tumours were defined by high immune cell infiltration and abundance of endothelial cells. Additionally, TME^{High} tumours are enriched for markers associated with T cell activation, MHC I genes, myeloid cell chemotaxis, inhibitory T cells, regulatory T cells, tumour associated macrophage and Immune checkpoints. These markers are indicative of a highly immunosuppressive, tumour-promoting environment[39,40]. Targeting specific cell populations to alleviate immunosuppression in TME^{High} GBM will likely be required to maximize response to immunotherapy. Interestingly, 65% of TME^{High} tumours were identified as Mes, suggesting that a subpopulation of Mes patients may respond to ICI, with TME subtyping representing a more refined predictive classification approach. TME subtype analysis of IvyGAP anatomical samples revealed TME^{High} patients comprised the highest proportion of samples defined as ‘microvascular proliferation’ regions, a classical hallmark of GBM. DEGs and GO analysis in TME^{High} tumours further revealed several upregulated genes and pathways related to immunoregulation. Interestingly, TLSs (and an associated transcriptomic signature) were specifically identified in TME^{High}/mesenchymal+ tumours. TLSs have been associated with clinical benefit and response to immunotherapy in solid tumours[41], however the clinical relevance of TLSs in GBM remains unclear[42]. Our data suggests that monocytic lineage abundance may

influence mechanisms which impact OS of TLS^{High} patients. The immunosuppressive role of TAMs[27,43] and their role in inducing a mesenchymal-like state in GBM[44] is well documented. Thus, in TME^{High} GBM, TAMs may suppress TLS anti-tumour activity, hindering immunotherapy response. Future studies to confirm the promiscuity of TLSs and associated subsets of immunosuppressive macrophages in TME^{High} tumours is warranted[45]. Overall, our data suggests that targeting anti-PD1+anti-CTLA4, may be a viable approach although it is noteworthy that a previous Phase 1 trial identified concerning treatment related adverse effects (AEs) in rGBM patients treated with combinatorial nivolumab and ipilimumab therapy, followed by nivolumab monotherapy, Specifically, grade 3/4 AEs were reported in 90% of patients who received 1mg/kg nivolumab plus 3mg/kg ipilimumab (NIVO1+IPI3), and 30% of patients who received 3mg/kg nivolumab plus 1mg/kg ipilimumab (NIVO3+IPI1)[11]. A rational alternative strategy in this sub-cohort could be anti-PD1+TAM targeting (e.g. CSFR1 inhibitor).

Longitudinal assessment of TME-subtypes has also revealed their dynamic nature. Tumours which transitioned from TME^{Low} to TME^{Med} or TME^{High}, and TME^{Med} to TME^{High}, were associated with significantly enriched lymphocytes, myeloid population abundance, T-cell functionality and an immunosuppressive TME. Importantly, we and others have recently shown that IDHwt GBM recurrence may be attributed to increased immune cell composition, and presence of a myeloid cell state. Moreover, this enriched myeloid cell state is associated with a mesenchymal subtype shift [37]. Here we investigated whether TME subtypes are driven from a “lower to higher” TME status by changes in the neoplastic (Proliferative stem-like, Stem-like and Differentiated-like) and myeloid cell state upon

recurrence[37]. Our data suggests that TME^{Med} to TME^{High} switch is influenced by a distinct myeloid phenotype, decreased tumour cell differentiation and upregulated chemokine-signallingpathways. Moreover, CCL18 (promotes glioma progression) and ACP5 (mediator of glioma growth) were highly upregulated upon subtype switching.[46,47]. Overall, this pathway may harbour potential therapeutic avenues for the treatment of patients with tumours which transition from TME^{Med} to TME^{High} upon recurrence. To further understand subtype evolution and treatment resistance, scRNA-seq analysis and construction of dynamic cellular models to inform TME plasticity, cellular lineage and trajectory, is now required. It will also be important to consider whether therapeutic pressure may truly drive subtype switching[41,48]. Additional analyses of biopsies in primary and recurrent tumours (post-treatment) may further unravel the impact of intra-tumoural heterogeneity on TME-subtype classification and TME-subtype specific treatment resistance mechanisms[37].

Finally, the predictive potential of novel TME-subtypes was retrospectively assessed in interventional immunotherapy clinical trial datasets. Firstly, our analysis of the small Cloughesy trial dataset tentatively suggests that TME^{High} patients who receive neoadjuvant anti-PD1 might show improved OS compared to patients receiving adjuvant anti-PD1 alone. Nevertheless we acknowledge that TME stratification prior to neoadjuvant treatment is not without complexity. However, we hypothesize that in the future, TME subtyping might be performed prior to surgery by employing a blood based cell free RNA (cfRNA) liquid biopsy method[49], or a robust TME subtype specific MRI radiomic signature[50,51]. Secondly, analysis of the Zhao cohort suggests that TME^{High} tumour-bearing patients trend towards improved OS following anti-PD1 therapy. In a very limited subset

of matched samples collected pre- and post- ICI therapy (*N*=3 patients), no significant alterations were detected in MCP scores before or after treatment (Supplementary Figure 17). As mentioned above, conclusions with respect to subtype switching may not be drawn from such a limited number of samples. Thus, further studies in expanded patient cohorts are now warranted. Interestingly, a relationship between TME subtype assigned at time of primary tumour resection and response to anti-PD1 was observed regardless of standard of care treatment regimen prior to anti-PD1 therapy. This observation also requires further validation. Thirdly, we investigated whether TME-subtypes were predictive of survival within the small PSVRIPO dataset (NCT01491893). Here, GBM patients received adjuvant anti-PD1 (newly diagnosed) or PVSRIPO therapy (recurrent tumours, treatment administered post biopsy). Stratification of PVSRIPO patients based on TME-subtypes suggest a trend towards improved OS in TME^{High} patients, compared with TME^{Med} and TME^{Low} patients. Clearly these hypothesis generating data now require validation in larger clinical cohorts. Desjardins have recently shown that a low mutational burden was associated with increased tumor-intrinsic inflammation in rGBM and increased response to PVSRIPO treatment[52]. Interestingly, our data suggests that TME^{High} patients may harbour a lower mutational burden than other subtypes, yet represent the subtype with the highest proportion of ICI responders.

Overall as mentioned, while we observe promising trends in all trial cohorts assessed, sample numbers are limited. Moreover, each trial cohort analysed has a unique study design and implements a specific immunotherapy regimen. Furthermore, an important study limitation is that validation of our findings in an expanded cohort of samples from

recently conducted negative Phase III trials (e.g. Checkmate-143, Checkmate-548 and Checkmate-498) has not been possible due to lack of availability of tissue/ RNAseq data. A tailored, Phase 2 study employing a rational hypothesis- driven trial design is now required to validate our findings. This trial should mandate for the robust collection of fresh frozen tissue for retrospective molecular analysis.

In conclusion, our multi-centre study introduces novel TME-subtypes which may inform optimal precision immunotherapy treatment strategies in the GBM setting. Our data provides convincing evidence that a TME-subtype classification system represents a canonical "*terminus a quo*" (starting point) to (i) deepen knowledge of GBM TME biology, (ii) support identification of patient subgroups who may benefit from immunotherapy and/or other TME targeting agents and (iii) provide a platform for the identification of new TME-associated contexts of vulnerability. Our findings warrant further investigation in additional retrospective immunotherapy trial cohorts, and in the prospective setting.

Acknowledgements

The work presented in this paper is dedicated to the memory of Mr Paolo Iacovelli. We would like to thank J. Heffernan, L.M Houlihan and J. Mythen (Beaumont Hospital Neuropathology Dept) for their help in establishing the GLIOTRAIN biobank in Dublin. The authors gratefully acknowledge all patients who kindly donated tumour tissue and clinical/ genomic data used in this study.

Funding information

This project has received funding from the European Union's Horizon 2020 research and innovation programme under the Marie Skłodowska-Curie ITN initiative (Grant Agreement #766069, GLIOTRAIN (http://www.gliotrain.eu) and 'GLIORESOLVE' projects (Grant Agreement #101073386). Additional support was received by donation from the Paolo Iacovelli memorial endowment. We are also grateful for financial support from the Beaumont Hospital Foundation, and from Brain Tumour Ireland to establish the Beaumont Hospital Brain Tumour Biorepository. The authors further acknowledge financial contribution towards staff salaries from RCSI and Champions Oncology (Baltimore, US).

Disclosure

The authors declare no conflict of interest. The funders had no role in the design of the study; in the collection, analyses, or interpretation of data; in the writing of the manuscript, or in the decision to publish the results.

Bibliography

1. Brat DJ, Aldape K, Colman H, Figrarella-Branger D, Fuller GN, Giannini C, et al. cIMPACT-NOW update 5: recommended grading criteria and terminologies for IDH-mutant astrocytomas. *Acta Neuropathol*. March 1, 2020;139(3):603–608.
2. White K, Connor K, Clerkin J, Murphy BM, Salvucci M, O'Farrell AC, et al. New hints towards a precision medicine strategy for IDH wild-type glioblastoma. *Annals of Oncology*. September 2020;
3. Schiffer D, Annovazzi L, Casalone C, Corona C, Mellai M. Glioblastoma: Microenvironment and niche concept. Vol. 11, Cancers. MDPI AG 2019.
4. Berghoff AS, Kiesel B, Widhalm G, Rajky O, Ricken G, Wöhrer A, et al. Programmed death ligand 1 expression and tumor-infiltrating lymphocytes in glioblastoma. *Neuro Oncol*. August 2015 [cited November 29, 2017];17(8):1064–1075. Available at: http://www.ncbi.nlm.nih.gov/pubmed/25355681
5. Nduom EK, Wei J, Yaghi NK, Huang N, Kong L-Y, Gabrusiewicz K, et al. PD-L1 expression and prognostic impact in glioblastoma. *Neuro Oncol*. February 2016

[cited November 29, 2017];18(2):195–205. Available at: http://www.ncbi.nlm.nih.gov/pubmed/26323609

6. Preusser M, Lim M, Hafler DA, Reardon DA, Sampson JH. Prospects of immune checkpoint modulators in the treatment of glioblastoma. *Nat Rev Neurol*. September 11, 2015;11(9):504–514. Available at: http://www.nature.com/articles/nrneurol.2015.139
7. Reardon DA, Gokhale PC, Klein SR, Ligon KL, Rodig SJ, Ramkissoon SH, et al. Glioblastoma Eradication Following Immune Checkpoint Blockade in an Orthotopic, Immunocompetent Model. *Cancer Immunol Res*. February 1, 2016 [cited November 29, 2017];4(2):124–135. Available at: http://www.ncbi.nlm.nih.gov/pubmed/26546453
8. Yuan B, Wang G, Tang X, Tong A, Zhou L. Immunotherapy of glioblastoma: recent advances and future prospects. *Hum Vaccin Immunother*. March 28, 2022;1–16.
9. Reardon DA, Brandes AA, Omuro A, Mulholland P, Lim M, Wick A, et al. Effect of Nivolumab vs Bevacizumab in Patients with Recurrent Glioblastoma: The CheckMate 143 Phase 3 Randomized Clinical Trial. *JAMA Oncol*. 2020;6(7):1003–1010.
10. Bristol Myers Squibb. Bristol Myers Squibb: Checkmate-548 [Internet]. 2019 [cited April 21, 2022]. Available at: https://tinyurl.com/j6v2zkkj
11. Omuro A, Vlahovic G, Lim M, Sahebjam S, Baehring J, Cloughesy T, et al. Nivolumab with or without ipilimumab in patients with recurrent glioblastoma: Results from exploratory phase i cohorts of CheckMate 143. *Neuro Oncol*. 2018;20(5):674–686.
12. Bristol-Myers Squibb. Bristol-Myers Squibb Announces Phase 3 CheckMate -498 Study Did Not Meet Primary Endpoint of Overall Survival with Opdivo (nivolumab) Plus Radiation in Patients with Newly Diagnosed MGMT-Unmethylated Glioblastoma Multiforme. 2019 [cited May 4, 2022]; Available at: https://news.bms.com/news/corporate-financial/2019/Bristol-Myers-Squibb-Announces-Phase-3-CheckMate--498-Study-Did-Not-Meet-Primary-Endpoint-of-Overall-Survival-with-Opdivo-nivolumab-Plus-Radiation-in-Patients-with-Newly-Diagnosed-MGMT-Unmethylated-Glioblastoma-Multiforme/default.aspx
13. Cloughesy TF, Mochizuki AY, Orpilla JR, Hugo W, Lee AH, Davidson TB, et al. Neoadjuvant anti-PD-1 immunotherapy promotes a survival benefit with intratumoral and systemic immune responses in recurrent glioblastoma. *Nat Med*. March 11, 2019;25(3):477–486. Available at: http://www.nature.com/articles/s41591-018-0337-7
14. Becht E, Giraldo NA, Lacroix L, Buttard B, Elarouci N, Petitprez F, et al. Estimating the population abundance of tissue-infiltrating immune and stromal cell populations using gene expression. *Genome Biol*. December 20, 2016 [cited March 25, 2019];17(1):218. Available at: http://genomebiology.biomedcentral.com/articles/10.1186/s13059-016-1070-5
15. McLendon R, Friedman A, Bigner D, van Meir EG, Brat DJ, Mastrogianakis GM, et al. Comprehensive genomic characterization defines human glioblastoma genes and core pathways. *Nature*. October 23, 2008;455(7216):1061–1068. Available at: http://www.nature.com/articles/nature07385

16. Zhao Z, Zhang KN, Wang Q, Li G, Zeng F, Zhang Y, et al. Chinese Glioma Genome Atlas (CGGA): A Comprehensive Resource with Functional Genomic Data from Chinese Glioma Patients. *Genomics Proteomics Bioinformatics*. February 1, 2021;19(1):1–12.
17. Aldape K, Amin SB, Ashley DM, Barnholtz-Sloan JS, Bates AJ, Beroukhim R, et al. Glioma through the looking GLASS: Molecular evolution of diffuse gliomas and the Glioma Longitudinal Analysis Consortium. *Neuro Oncol*. 2018;20(7):873–884.
18. Zhao J, Chen AX, Gartrell RD, Silverman AM, Aparicio L, Chu T, et al. Immune and genomic correlates of response to anti-PD-1 immunotherapy in glioblastoma. *Nat Med*. March 11, 2019;25(3):462–469. Available at: http://www.nature.com/articles/s41591-019-0349-y
19. Desjardins A, Gromeier M, Herndon JE, Beaubier N, Bolognesi DP, Friedman AH, et al. Recurrent Glioblastoma Treated with Recombinant Poliovirus. *New England Journal of Medicine*. July 12, 2018;379(2):150–161.
20. Klemm F, Maas RR, Bowman RL, Kornete M, Soukup K, Nassiri S, et al. Interrogation of the Microenvironmental Landscape in Brain Tumors Reveals Disease-Specific Alterations of Immune Cells. *Cell*. 2020;181(7):1643-1660.e17. Available at: https://doi.org/10.1016/j.cell.2020.05.007
21. Wang Q, Hu B, Hu X, Kim H, Squatrito M, Scarpace L, et al. Tumor Evolution of Glioma-Intrinsic Gene Expression Subtypes Associates with Immunological Changes in the Microenvironment. *Cancer Cell*. July 2017;32(1):42-56.e6.
22. Nehama D, di Ianni N, Musio S, Du H, Patané M, Pollo B, et al. B7-H3-redirected chimeric antigen receptor T cells target glioblastoma and neurospheres. *EBioMedicine*. September 1, 2019;47:33–43.
23. Zhang J, Wang J, Marzese DM, Wang X, Yang Z, Li C, et al. B7H3 regulates differentiation and serves as a potential biomarker and theranostic target for human glioblastoma. *Laboratory Investigation*. July 1, 2019;99(8):1117–1129.
24. Zhang C, Zhang Z, Li F, Shen Z, Qiao Y, Li L, et al. Large-scale analysis reveals the specific clinical and immune features of B7-H3 in glioma. *Oncoimmunology*. November 2, 2018;7(11).
25. Digregorio M, Coppieters N, Lombard A, Lumapat PN, Scholtes F, Rogister B. The expression of B7-H3 isoforms in newly diagnosed glioblastoma and recurrence and their functional role. *Acta Neuropathol Commun*<="" span="">
26. Coppola D, Nebozhyn M, Khalil F, Dai H, Yeatman T, Loboda A, et al. Unique ectopic lymph node-like structures present in human primary colorectal carcinoma are identified by immune gene array profiling. *American Journal of Pathology*. July 2011;179(1):37–45.
27. Sautès-Fridman C, Petitprez F, Calderaro J, Fridman WH. Tertiary lymphoid structures in the era of cancer immunotherapy. Vol. 19, Nature Reviews Cancer. Nature Publishing Group 2019; 307–325.
28. Preusser M, Lim M, Hafler DA, Reardon DA, Sampson JH. Prospects of immune checkpoint modulators in the treatment of glioblastoma. *Nat Rev Neurol*. 2015;11(9):504–514.
29. Schalper KA, Rodriguez-Ruiz ME, Diez-Valle R, López-Janeiro A, Porciuncula A, Idoate MA, et al. Neoadjuvant nivolumab modifies the tumor immune microenvironment in resectable glioblastoma. *Nat Med*. 2019;25(3):470–476.

30. Lee AH, Sun L, Mochizuki AY, Reynoso JG, Orpilla J, Chow F, et al. Neoadjuvant PD-1 blockade induces T cell and cDC1 activation but fails to overcome the immunosuppressive tumor associated macrophages in recurrent glioblastoma. *Nat Commun*. December 1, 2021;12(1).
31. Kan LK, Drummond K, Hunn M, Williams D, O'Brien TJ, Monif M. Potential biomarkers and challenges in glioma diagnosis, therapy and prognosis. Vol. 2, BMJ Neurology Open. BMJ Publishing Group 2020.
32. Zhang J, Sai K, Wang X li, Ye S quan, Liang L jiao, Zhou Y, et al. Tim-3 Expression and MGMT Methylation Status Association With Survival in Glioblastoma. *Front Pharmacol*. September 15, 2020;11.
33. Nathanson DA, Gini B, Mottahedeh J, Visnyei K, Koga T, Gomez G, et al. Targeted therapy resistance mediated by dynamic regulation of extrachromosomal mutant EGFR DNA. *Science (1979)*. 2014;343(6166):72–76.
34. Brat DJ, van Meir EG. Vaso-occlusive and prothrombotic mechanisms associated with tumor hypoxia, necrosis, and accelerated growth in glioblastoma. Vol. 84, Laboratory Investigation. 2004; 397–405.
35. Cheng X, Yin H, Fu J, Chen C, An J, Guan J, et al. Aggregate analysis based on TCGA: TTN missense mutation correlates with favorable prognosis in lung squamous cell carcinoma. *J Cancer Res Clin Oncol*. April 2, 2019;145(4):1027–1035.
36. Wu P, Yang W, Ma J, Zhang J, Liao M, Xu L, et al. Mutant-allele tumor heterogeneity in malignant glioma effectively predicts neoplastic recurrence. *Oncol Lett*. 2019;18(6):6108–6116.
37. Varn FS, Johnson KC, Martinek J, Huse JT, Nasrallah MP, Wesseling P, et al. Glioma progression is shaped by genetic evolution and microenvironment interactions. *Cell*. June 1, 2022;185(12):2184-2199.e16. Available at: https://linkinghub.elsevier.com/retrieve/pii/S0092867422005360
38. Johnson KC, Anderson KJ, Courtois ET, Gujar AD, Barthel FP, Varn FS, et al. Single-cell multimodal glioma analyses identify epigenetic regulators of cellular plasticity and environmental stress response. *Nat Genet*. October 1, 2021;53(10):1456–1468.
39. Togashi Y, Shitara K, Nishikawa H. Regulatory T cells in cancer immunosuppression — implications for anticancer therapy. *Nat Rev Clin Oncol*. Available at: https://doi.org/10.1038/s41571-
40. Takenaka MC, Gabriely G, Rothhammer V, Mascanfroni ID, Wheeler MA, Chao CC, et al. Control of tumor-associated macrophages and T cells in glioblastoma via AHR and CD39. *Nat Neurosci*. May 1, 2019;22(5):729–740.
41. Neftel C, Laffy J, Filbin MG, Hara T, Shore ME, Rahme GJ, et al. An Integrative Model of Cellular States, Plasticity, and Genetics for Glioblastoma. *Cell*. 2019;178(4):835-849.e21.
42. van de Walle T, Vaccaro A, Ramachandran M, Pietilä I, Essand M, Dimberg A. Tertiary Lymphoid Structures in the Central Nervous System: Implications for Glioblastoma. Vol. 12, Frontiers in Immunology. Frontiers Media S.A. 2021.
43. Petitprez F, Lévy S, Sun CM, Meylan M, Linhard C, Becht E, et al. The murine Microenvironment Cell Population counter method to estimate abundance of tissue-

infiltrating immune and stromal cell populations in murine samples using gene expression. *bioRxiv*. 2020;

44. Hara T, Chanoch-Myers R, Mathewson ND, Myskiw C, Atta L, Bussema L, et al. Interactions between cancer cells and immune cells drive transitions to mesenchymal-like states in glioblastoma. *Cancer Cell*. June 2021;39(6):779-792.e11. Available at: https://linkinghub.elsevier.com/retrieve/pii/S1535610821002683
45. Goswami S, Walle T, Cornish AE, Basu S, Anandhan S, Fernandez I, et al. Immune profiling of human tumors identifies CD73 as a combinatorial target in glioblastoma. Vol. 26, Nature Medicine. Nature Research 2020; 39–46.
46. Huang Y, Motta E, Nanvuma C, Kuhrt LD, Yuan Y, Xia P, et al. Microglia/macrophage-derived human CCL18 promotes glioma progression via CCR8-ACP5 axis analyzed in humanized slice model. *Cell Rep*. April 12, 2022;39(2).
47. Grochans S, Korbecki J, Simińska D, Żwierełło W, Żeszotek S, Kolasa A, et al. CCL18 Expression Is Higher in a Glioblastoma Multiforme Tumor than in the Peritumoral Area and Causes the Migration of Tumor Cells Sensitized by Hypoxia. *Int J Mol Sci*. August 1, 2022;23(15).
48. Chaligne R, Gaiti F, Silverbush D, Schiffman JS, Weisman HR, Kluegel L, et al. Epigenetic encoding, heritability and plasticity of glioma transcriptional cell states. *Nat Genet*. October 1, 2021;53(10):1469–1479.
49. Müller Bark J, Kulasinghe A, Chua B, Day BW, Punyadeera C. Circulating biomarkers in patients with glioblastoma. Vol. 122, British Journal of Cancer. Springer Nature 2020; 295–305.
50. Zhang Z, He K, Wang Z, Zhang Y, Wu D, Zeng L, et al. Multiparametric MRI Radiomics for the Early Prediction of Response to Chemoradiotherapy in Patients With Postoperative Residual Gliomas: An Initial Study. *Front Oncol*. November 18, 2021;11.
51. Park JE, Kim HS, Jo Y, Yoo RE, Choi SH, Nam SJ, et al. Radiomics prognostication model in glioblastoma using diffusion- and perfusion-weighted MRI. *Sci Rep*. December 1, 2020;10(1).
52. Gromeier M, Brown MC, Zhang G, Lin X, Chen Y, Wei Z, et al. Very low mutation burden is a feature of inflamed recurrent glioblastomas responsive to cancer immunotherapy. *Nat Commun*. December 2021;12(1):1–7.

Figure Legends

Figure 1. Identification and validation of novel TME subtypes in GLIOTRAIN cohort and validation datasets (TCGA, CGGA, DUKE). A. Partition around medoids (PAM) clustering of the GLIOTRAIN cohort (N=123), based on the cellular TME composition described by MCP-counter scores reveals 3 subgroups; TMElow, TMEmed and TMEhigh in the B. TCGA, C. CCGA and D. DUKE cohorts E. OS according to TMElow, TMEmed and TMEhigh subtypes in the GLIOTRAIN cohort (P=0.55), F. TCGA cohort (P=0.53), G. CGGA cohort (P=0.13) and H. Duke cohort (P=0.55). I. Proportion of Wang subtypes22 in the TME classifiers. Statistical test A-D: Kruskal Wallis one-way analysis of variance. E-H: P value of log-ranked test. CL: Classical, Mes: Mesenchymal, PN: Proneural.

Figure 2. Characterisation of TME subtype specific biology. A. TME functional orientation markers and immune checkpoint expression across TME subtypes in the GLIOTRAIN discovery cohort. B. Neoantigen prediction across the TME subtypes in the TCGA cohort C. Mutation frequency across the TME subtypes in the TCGA cohort. D. TME subtype-specific mutation frequency for the top 10 genes with highest frequency in the TCGA cohort. E. Volcano plots showing differentially expressed genes in TME^{Low}, F. TME^{Med} and G. TME^{High} patients. Statistical test B,C: Kruskal Wallis one-way analysis of variance.

Figure 3. GBM TME and associated TME subtypes exhibit cellular heterogeneity upon recurrence. A. Heatmap showing the expression of GBM-MCP scores, FO markers and immune checkpoints in Primary tumours (TP), first recurrence (R1) and combined second, third and fourth recurrence in the GLASS cohort. B. Continuous bar graph showing the distribution of TME subtypes in matching primary and recurrent tumours (*N*=99 tumour pairs). C. Sankey plot indicating the transition of TME subtypes on recurrence. Band size reflects sample numbers and band colours represent TME subtype. D. Boxplots showing the TME cell populations with significantly enriched MCP-scores from primary to recurrent samples in patients who switch subtype; D. TME^{Low} (primary) to TME^{Med} (recurrent) tumours, E. TME^{Low} (primary) to $TMEHi^{gh}$ (recurrent) tumours and F. TME^{Med} (primary) to TME^{High} (recurrent) tumours. Statistical test: Wilcoxon signed rank test. * P<0.05 ***P<0.001

Figure 4. Trend towards improved OS following neoadjuvant pembrolizumab in recurrent IDHwt GBM TMEhigh patients. A. Partition around medoids (PAM) clustering of IDHwt GBM samples in the Cloughesy cohort13 with available RNA-seq data (*N*=23), based on the cellular TME composition described by GBM-MCP-counter scores reveal 3 subtypes; TME^{Low}, TME^{Med} and TME^{High}. B. OS according to TME^{Low}, TME^{Med} and TME^{High} subtypes in the Cloughesy cohort C. OS according to TMELow/neoadjuvant anti-PD-1, TMEMed/adjuvant anti-PD-1, TMEHigh/adjuvant anti-PD-1 and TMEHigh/adjuvant patients in the Cloughesy cohort. TMEMed patients treated with neoadjuvant anti-PD1 (*N*=1) and TME^{Low} patients treated with adjuvant anti-PD1 (*N*=2) were excluded due to small patient numbers D. Boxplot representing OS of patients in the Cloughesy cohort. Boxplots are colour coded according to the patients TME subtype and whether they received Neoadjuvant + adjuvant (Neo) anti-PD1 therapy or adjuvant (Adj) anti-PD1 alone. Orange; $TME^{High/Adj}$, Gold; $TME^{High/Neo}$, Green; $TME^{Low/Adj}$, Light blue; $TME^{Low/Neo}$, Dark blue;

TME$^{Med/Adj}$ and pink; TME$^{Med/Neo}$. Statistical test: Kaplan Meier analysis; P value of log-ranked test.

Figure 5. Trend towards improved OS and increased response rate in TME^{High} patients following adjuvant treatment with pembrolizumab or PVSRIPO . A. TME composition in Zhao dataset[18] pre- vs post- adjuvant anti-PD1 treatment in available tumour (*N*=24) samples. B. OS according to TME^{High} and non-TME^{High} (TME^{Low} + TME^{Med}) subtypes who received adjuvant anti-PD1 therapy in the Zhao cohort (*N*=15 patients). C. Relative boxplots indicating the proportion of TME^{Low,} TME^{Med} and TME^{High} patients before administration of anti-PD1 treatment (left) and after anti-PD1 treatment (right) in available tumour and blood samples. D. Partition around medoids (PAM) clustering of the PVSRIPO cohort[19] with available RNA-seq data (*N*=12), based on the cellular TME composition described by GBM-MCP-counter scores reveal 3 subtypes; TME^{low}, TME ^{med} and TME ^{high}. E. OS according to TME^{Low} and TME^{Med} and TME^{High} subtypes who received PVSRIPO therapy in the PVSRIPO cohort[19]. Statistical test: Wilcoxon signed rank test. Kaplan Meier analysis; P value of log-ranked test. **P*<0.05 ** *P*<0.01

Supplementary Figure 1. GBM dataset filtering process for the GLIOTRAIN cohort (discovery), TCGA, CGGA, and Duke cohorts (validation), the GLASS longitudinal cohort, IvyGAP cohort, Cloughesy, Zhao and PVSRIPO cohorts (Immunotherapy clinical trial cohorts).

Supplementary Figure 2. Refinement and immunohistochemical validation of MCP-counter for application in GBM. A. Representative images of the IHC and IF panel employed for MCP validation and authentication of GBM specific microglial signature. B. Correlation of GBM-MCP-counter scores with corresponding cell densities measured by IHC. Statistical analysis B: Spearman's rank correlation coefficient

Supplementary figure 3. Confirmation of novel TME subtypes as three distinct non-overlapping biological entities**. A.** Principle component analysis clustering of the TME^{Low}, TME^{Med} and TME^{High} subtypes in the GLIOTRAIN, **B.** TCGA, **C.** CGGA and **D.** DUKE cohorts.

Supplementary figure 4. Comparison of novel TME subtypes GBM-MCP scores in the **A.** GLIOTRAIN, **B.** TCGA **C.** CGGA and **D.** DUKE cohorts

Supplementary figure 5. Comparison of novel TME subtypes GBM-MCP scores in the A. GLIOTRAIN, B. TCGA C. CGGA and D. DUKE cohorts

Supplementary Figure 6. Immunohistochemical validation of TME subtypes. A. Partition around medoids (PAM) clustering of GLIOTRAIN "IHC sub-cohort" (*N*=26). GBM-MCP-counter scores ascribes this validation cohort to TME $^{low, med, high}$ subtypes. B. Subtypes were further validated via IHC staining. Representative images demonstrating CD3/CD20, CD8/CD66b, CD68 and SMA/PD-L1/CD34 expression by IHC of TME $^{low, med, high}$ tumours. **C.** Cell density counts showing the differences in immune and stromal composition across TME subtypes. Scale bar: 100um. Statistical test C: Kruskal Wallis one-way analysis of variance.

Supplementary Figure 7. Survival analysis across Wang subtypes (PN, CL and Mes), in the A. GLIOTRAIN cohort, B. TCGA cohort and C. CGGA cohort. Statistical test A-C: Kaplan Meier analysis; P value of log-ranked test.

Supplementary Figure 8. Characterisation of TME subtype specific biology in validation cohorts. A. Functional orientation and immune checkpoint expression of the TME sub-groups in the A. TCGA cohort, B. CGGA cohort and C. DUKE cohort.

Supplementary Figure 9. Tertiary Lymphoid structures (TLSs) and the 12-chemokine TLS signature may be a feature of TME^{High} GBM A. TLS aggregates are observed in TME^{High} tumours (*N*=3) in the GLIOTRAIN "IHC sub-cohort" via IHC (CD20/CD3). B. Heat map demonstrating expression of T cells, CD8 T cells, B lineage, NK cells and TLS-associated 12-chemokine signature across subtypes. C. Assessment of survival in GLIOTRAIN cohort (*N*=123) based on TLS signature expression. No significant different is observed in OS of GBM patients according to TLS signature expression (*P*=0.095). TLS High and low subgroups were calculated based on median threshold of TLS signature. D. Assessment of survival in GLIOTRAIN cohort (*N*=123) based on TLS and monocytic lineage signature expression. OS of patients based on the TLS-signature and monocytic lineage abundance. Tumours were classified as TLS signature High and monocytic lineage High based on median threshold**.** Monocytic $lineage^{High}/TLS^{Low}$ GBMs display a trend towards poorer OS (*P*=0.011). **E.** Gene expression heatmap of antigen-presenting cell (APC) and T cell activating and inhibitory signalling mediators in TLS^{Low} and TLS^{High} subgroups in GLIOTRAIN cohort (*N*=123). Scale bars: 500um. Statistical test C,D: Kaplan Meier analysis; P value of log-ranked test.

Supplementary figure 10. Comparison of MGMT methylation status across the TME subtypes in A. GLIOTRAIN, B. TCGA, C. CGGA and D. Duke cohorts

Supplementary Figure 11. Gene Ontology (GO) analysis in TME^{Low}, TME^{Med} and TME^{High} subtypes (GLIOTRAIN cohort). GO analysis showing the 10 most upregulated pathways (Bioplanet 2019) in A. TME^{Low}, B. TME^{Med} and C. TME^{High} subtypes.

Supplementary Figure 12. Gene Ontology (GO) analysis in TME^{Low}, TME^{Med} and TME^{High} subtypes (GLIOTRAIN cohort). GO analysis showing the 10 most downregulated pathways (Bioplanet 2019) in A. TME^{Low}, B. TME^{Med} and C. TME^{High} subtypes.

Supplementary Figure 13. Histological features correlate to TME subtype distribution. A. Partition around medoids (PAM) clustering of the Ivy GAP GBM cohort (n=10 patients), based on the cellular TME composition described by MCP-counter scores reveal 3 subgroups; TME low, TME med and TME high in the Ivy GAP cohort. B. Distribution of TME subtypes based on Ivy GAP histological features.

Supplementary Figure 14. Longitudinal analysis of TME subtypes and TME composition upon recurrence (GLASS cohort). Heatmap of GBM-MCP cell distribution in primary and recurrent IDHwt GBM samples from the GLASS cohort ([17] n=99 tumour pairs). B.

Boxplots showing significant changes in GBM-MCP score when samples 'switch' from B. TME^{Med} to TME^{Low} and C. TME^{High} to TME^{Med} upon recurrence. D. Sankey plot indicating the transition of TME subtypes on recurrence based on immunotherapy treatment. Band size reflects sample numbers and band colours represent TME subtype. Statistical test: Wilcoxon signed rank test.

Supplementary Figure 15. Cell-state changes and upregulated chemokine pathways are associated with TME subtype transitions upon recurrence. A. Boxplots showing the non-neoplastic cell-states (Myeloid) and neoplastic cell-states (Prolif stem-like, Stem-like and Diff-like) from primary to recurrent samples in patients who switch subtype; TME^{Low} (primary) to TME^{Med} (recurrent) tumours, B. TME^{Low} (primary) to TME^{High} (recurrent) tumours and C. TME^{Med} (primary) to TME^{High} (recurrent) tumours. D. GO analysis showing the 10 most upregulated pathways (Bioplanet 2019) in samples which transitioned from TME^{Med} to TME^{High} upon recurrence. E. Volcano plots showing differentially expressed genes in samples which transitioned from TME^{Med} to TME^{High} upon recurrence. Statistical test: Wilcoxon signed rank test.

Supplementary Figure 16. Comparison of GBM-MCP scores and TME subtype distribution in non-responders and responders in the Zhao cohort A. GBM-MCP scores categorized based on non-responders and responders in the Zhao cohort. B Relative bargraph indicating the proportion of $TME^{Low,}$ TME^{Med} and TME^{High} patients who are classified as Non-responders (left) and responders (right) according to Zhao et al., in available tumour samples.

Supplementary Figure 17. Comparison of TME composition in patients with matched pre- and post anti-PD1 treated samples. A. MCP scores categorized based on patients with matched Pre anti-PD1 treated and post-anti-PD1 treated samples in the Zhao cohort (*N*=3).

‡Annex I

GLIOTRAIN Consortium

- Martine Lamfers - m.lamfers@erasmusmc.nl
- Sieger Leenstra - s.leenstra@erasmusmc.nl
- Ioannis Ntafoulis - i.ntafoulis@erasmusmc.nl
- Federica Fabro - f.fabro@erasmusmc.nl
- JM Kros - j.m.kros@erasmusmc.nl

- Emie Quissac - Emie.quissac@icm-institute.org
- Archita Biswas - architabiswas@rcsi.ie
- J Cryan - janecryan@beaumont.ie
- F Brett - francescabrett@beaumont.ie
- A Beausang - alanbeausang@beaumont.ie
- S MacNally - stephenmacnally@beaumont.ie
- Phil O'Halloran - philohalloran@rcsi.ie
- James Clerkin - jamesclerkin@rcsi.ie
- Orna Bacon - ornabacon@gmail.com
- Diether Lambrechts - diether.lambrechts@kuleuven.be
- Gonca Dilcan - gonca.dilcandurdag@kuleuven.be
- Francesca Lodi - francesca.lodi@kuleuven.be
- Ingrid Arijs - ingrid.arijs@kuleuven.be
- Andreas Kremer - andreas.kremer@ittm-solutions.com
- Romain Tching Chi Yen - romain.tching@ittm-solutions.com

1

[1] Referred to throughout as “GBM” based on recent c-IMPACT-NOW[1] recommendations

Highlights:

1. Studying the *IDH*-wt GBM tumour microenvironment (TME) transcriptome reveals three distinct GBM subtypes; TME^{High},TME^{Med}, TME^{Low}.
2. Novel TME subtypes are dynamic and evolve across primary and recurrent GBMs.
3. Interrogation of retrospective trial datasets suggest that patient response to immunotherapies could be TME subtype specific

4. TME$^{High,\ Med,\ Low}$ GBMs manifest specific contexts of vulnerability which could direct novel combinatorial treatment strategies.
5. In the future, patient assignment to TME subtypes may support precision immunotherapy treatment in IDH-wt GBM.

Abstract

Background: New precision medicine therapies are urgently required for glioblastoma (GBM). However, to date, efforts to subtype patients based on molecular profiles, have failed to direct treatment strategies. We hypothesized that interrogation of the GBM tumor microenvironment (TME) and identification of novel TME specific subtypes could inform new precision immunotherapy treatment strategies.

Methods: A refined and validated microenvironment cell population (MCP)-counter method was applied to >800 GBM patient tumours (GBM-MCP-counter). Specifically, partition arounds medoids (PAM) clustering of GBM-MCP-counter scores in the GLIOTRAIN discovery cohort identified 3 novel patient clusters, uniquely characterised by TME-composition, functional orientation markers and immune checkpoint proteins. Validation was performed in three independent GBM-RNA-seq datasets. Neo-antigen, mutational, and gene ontology analysis identified mutations and uniquely altered pathways across subtypes. The longitudinal GLASS cohort and three immunotherapy clinical trial cohorts (treatment with neoadjuvant/adjuvant anti-PD1 or PSVRIPO) were further interrogated to assess subtype alterations between primary and recurrent tumours, and to assess the utility of TME classifiers as immunotherapy biomarkers.

Results: TME^{High} tumours (30%) displayed elevated lymphocyte, myeloid cell immune checkpoint, PDCD1(PD1) and CTLA4 transcripts. TME^{High}/mesenchymal+ patients featured tertiary lymphoid structures (TLS). TME^{Med} (46%) tumours were enriched for endothelial cell gene expression profiles and displayed heterogeneous immune populations. TME^{Low} (24%) tumours were manifest as an 'immune-desert' group. TME-subtype transitions upon recurrence were identified in the longitudinal GLASS cohort. Assessment of GBM immunotherapy trial datasets revealed that TME^{High} patients receiving neo-adjuvant anti-PD1 had significantly increased OS (P=0.04). Moreover, TME^{High} patients treated with adjuvant anti-PD1 or oncolytic virus (PVSRIPO), showed a trend towards improved survival.

Conclusions: We have established a novel TME-based classification system for application in intracranial malignancies. TME-subtypes represent canonical "*termini a quo"* (starting points) to support an improved precision immunotherapy treatment approach.

Introduction

Elucidation of IDHwt GBM[1] disease subtypes[1] based on mutational profiling, gene expression and DNA methylation has failed to translate into improved clinical outcomes[2]. GBM tumours are complex ecosystems composed of diverse malignant (e.g. stem) and non-malignant (e.g. glial, microglia, immune cells, vascular cells, reactive astrocytes) cell populations which exist in several niches, interact with heterogeneous tumour cells[3] and

exhibit a dynamic heterogeneity and plasticity. Of late, there has been much focus on targeting the GBM immune cell niche, notwithstanding a generalized immunosuppressive microenvironment in the intracranial setting. For example, as the immune checkpoint protein PD-L1 is expressed in GBM[4,5] and pre-clinical data[6,7] provided rationale for evaluation of immune checkpoint inhibitors (ICIs), multiple clinical studies have now been completed. Disappointingly, these trials have been negative[8–12] most likely as limited patient stratification methods were available to rationally select patients who might benefit most from treatment. Nevertheless, a small multicentre randomised control trial conducted in the setting of recurrent GBM (rGBM) suggests that neo-adjuvant anti-PD-1 blockade may elicit enhanced immune responses and survival benefits[13].

In the current study, the GLIOTRAIN consortium (www.gliotrain.eu), together with US collaborators, have interrogated tissue-infiltrating immune and stromal cell populations of selected GBM patients using a modified targeted microenvironment cell-population counter (MCP-counter) RNA-seq computational method[14]. Unsupervised partition around medoids (PAM) clustering identified three novel TME-associated subtypes designated TME^{low}, TME^{med}, and TME^{high} which have been validated in publicly available datasets. To provide insight into novel subtype-specific biology, we analyzed TME functional orientation markers and differentially expressed genes. Moreover, we performed mutational analysis and neoantigen prediction across novel subtypes, and have longitudinally assessed subtype switching events in primary and recurrent tumours. Finally, the capacity of novel TME-subtypes to predict outcome was assessed in retrospective immunotherapy clinical trial datasets. Our findings lay the foundation for a

novel subtyping approach which may be applied, to direct novel combinatorial immunotherapy strategies in the brain tumour setting.

Materials and Methods

Patient Series (N=867 samples, N=8 cohorts)

GLIOTRAIN Discovery cohort

Informed consent for use of multi-omics data and associated clinical annotation was obtained via appropriate institutional channels. The GLIOTRAIN cohort was comprised of 123 retrospectively collected fresh frozen (FF) GBM samples, acquired at time of surgery, with corresponding clinical follow-up data. Patient samples were collected based on the GLIOTRAIN biobank inclusion criteria (Table 1). FF tumour samples from three participating institutions were collected (Table 2) and clinical data associated with GLIOTRAIN samples are described in Table 3.

Validation and Glioma Longitudinal Analysis Consortium (GLASS) Longitudinal Cohorts

Transcriptomic and clinical data from the Cancer Genome Atlas Glioblastoma Multiforme (TCGA-GBM) data collection was downloaded from the National Cancer Institute Genomic Data Commons (GDC) data portal (TCGA RNA-seq cohort)[15]. mRNAseq_693 (batch 1) dataset and clinical data was downloaded from the Chinese Glioma Atlas database (http://www.cgga.org.cn)(CGGA RNA-seq cohort)[16]. The DUKE cohort comprised GBM patients treated at Duke's Preston Robert Tisch Brain Tumor Center (RNA sequencing performed by Caris Life Sciences). The GLASS dataset (GLASS

cohort) was downloaded from Synapse (https://www.synapse.org/#!Synapse:syn17038081/wiki/585622)[17].Clinical annotation for DUKE and GLASS datasets provided from collaborators upon request and described in Table 3 and 4 respectively.

Immunotherapy Trial Cohorts

Transcriptomic data for GSE121810 were provided upon request (Cloughesy cohort[13]). Transcriptomic data was downloaded from SRAPRJNA482620 (Zhao cohort[18]). RNAseq bam files for the PVSRIPO clinical trial were downloaded from Genotypes and Phenotypes (dbGaP) database (PVSRIPO cohort). Clinical annotation for all datasets was also provided. [19] (Table 5 and 6). Discovery, validation, GLASS longitudinal and immunotherapy clinical trial cohorts were filtered as outlined (Supplementary figure 1).

For detailed descriptions of next generation sequencing methods, MCP-counter modification, interrogation of TME composition and validation of novel TME subtypes, Wang subtype classification, neoantigen prediction, multiplexed immunohistochemistry methods, IvyGAP dataset analysis, gene ontology analysis and statistical methods, see supplementary materials, at *Annals of Oncology* online.

Results

Modification and Validation of MCP-counter for application in GBM

We first established the MCP-counter method for application in GBM (GBM-MCP-counter). Specifically, we removed fibroblast scores, and a GBM-specific microglial signature described by KLEMM et al[20], was incorporated. Next, we validated GBM specific

gene expression at the protein level by IHC and IF (Supplementary Figure 2A). Correlations between GBM-MCP scores of immune cell populations and corresponding IHC cell density (Supplementary Figure 2B) were confirmed. CD3 T cells, CD8 T cells and monocyte lineage showed high correlation coefficients with IHC protein cell density evaluations (R= 0.43, 0.52, and 0.44, *P*=0.031, 0.012 and 0.048 respectively). Microglia expression signature significantly correlated with microglia IF panel cell density (CD68-/Iba1+/TMEM119) (*R*=0.56, *P*=0.0047) (Supplementary Figure 2B).

Identification of novel TME-subtypes

Partition around medoids (PAM) clustering, based on patient GBM-MCP-counter scores, was performed on the GLIOTRAIN cohort. Clustering identified 3 distinct, novel subtypes with significantly different TME compositions (silhouette statistic methods and principal component analysis (PCA) (Supplementary Figure 3A-D). These subgroups were defined as TME^{Low}, 'Immune-Low', (24%), TME^{Med}, 'heterogeneous immune populations', (46%) and TME^{High}, 'Immune-High' (30%) (Figure 1A). These findings were reproduced in TCGA, CGGA and DUKE datasets (Figure 1B-D, Supplementary Figure 4, Supplementary Figure 5). A representative cohort (*N*=26), from /span>GLIOTRAIN (GLIOTRAIN-IHC cohort) was assigned to TME-subtypes (Supplementary Figure 6A) and quantitative IHC data orthogonally validated each TME-subtype (Supplementary Figure 6B,C)[14]. Overall, GBM-MCP-counter analysis revealed that TME^{High} cases are characterized by significantly increased expression of genes specific to all immune populations (Figure 1A-D). TME^{Med} cases were characterised by high endothelial cell GBM-MCP signature, and

heterogeneous abundance of immune cells. Notably, the microglial signature was enriched in both TME^{High} and TME^{Med} subtypes (Figure 1A). Finally, the TME^{Low} subtype was characterised by a low expression of all immune and endothelial cell markers (Figure 1A-D). Stratification into TME^{High}, TME^{Med} or TME^{Low} subtypes showed no association with OS in GLIOTRAIN, TCGA, CGGA and DUKE cohorts (*P*=0.55, *P*=0.53, *P*=0.13, and *P*=0.55 respectively)(Figure 1E-H).

We subsequently studied the association of proneural (PN), classical (CL) and mesenchymal (Mes) gene expression subtypes[21] with novel TME-subtypes identified. TME^{High} tumours comprised of 23% PN, 18% CL and 59% Mes cases. TME^{Med} were comprised of 41% PN, 26% CL and 33% Mes, and TME^{Low} 55% CL, 35% PN and 10% Mes (Figure 1I). Findings remained consistent across all validation cohorts (Figure1B-D). Survival analysis following Wang subtype patient stratification[21] (PN, CL, Mes) showed no significant impact on OS in any cohort (Supplementary Figure 7A-C).

Biological characterisation of TME-subtypes

Next, we studied TME composition and functionality across subtypes. Expression of genes associated with functional orientation markers were significantly enriched in the TME^{High} subtype (Figure 2A) in the GLIOTRAIN cohort. Angiogenesis signature expression was homogenous across all TME-subtypes (*P*=0.38)(Figure 2A). The expression of immune-checkpoint-related genes showed a similar trend to immune infiltrate genes, with high expression of genes encoding PD1 and CTLA4 observed in the TME^{High} subtype (*P*=2.1e-05, *P*=1.4e-06)(Figure 2A). *CD274* (which encodes PDL1) was significantly

enriched in TME^{High} GBM and heterogeneously expressed across all TME-subtypes (*P*=0.0053), whereas *TIM3* was homogenously expressed across all subtypes (Figure 2A, Supplementary Figure 5A-C). Notably, B7 homolog 3 protein (B7-H3/CD276[22]) expression was significantly downregulated in TCGA cohort TME^{High} patients (*P*=0.012; Figure S7A). No significant difference in B7-H3 expression was observed across novel TME subgroups in other cohorts (Figure 2A, Supplementary Figure 8B, C). Interestingly, several previous studies assessing B7-H3 expression in GBM have observed similar diverse expression patterns[23–25].

We further interrogated TME-subtype mutational landscape within the TCGA RNA-seq cohort, where matching WES data were available. As expected, tumour mutational burden (TMB) was low (median: 48 mutations)[Data not shown]. Moreover, mutational analysis revealed no difference in neo-antigen prediction or mutation count across TME-subtypes (Kruskal-Wallis, *P*=0.14 and *P*=0.081 respectively)(Figure 2B,C). Nevertheless, a small number of genes were frequently mutated in specific TME-subtypes. Specifically, *EGFR* was most frequently mutated in TME^{Low} GBM, *TTN* in TME^{Med} and *PTEN* in TME^{High} tumours (Figure 2D). Interestingly, IHC analyses (CD20+/CD3+), revealed tertiary lymphoid structures (TLS) as a possible feature of TME^{High}/Mesenchymal^{+} GBM (Supplementary Figure 9A, B). Survival analysis in the GLIOTRAIN cohort based on TLS associated 12-chemokine signature[26,27] suggested monocytic lineage in TLS^{High} patients display suppressed immune responses (Supplementary figure 9C, D). Furthermore, TLS^{High} patients displayed enriched genes associated with T-cell activation and may therefore be able to elicit an immune response (Supplementary figure 9E). We also

analysed MGMT promoter methylation status across novel TME subtypes in the GLIOTRAIN, TCGA, CGGA and DUKE cohorts (Supplementary Figure 10). Overall, no significant relationship was observed between MGMT status and TME subtype.

Differential gene expression analysis across TME-subtypes revealed several significantly down-regulated genes in the TME^{Low} subtype when compared to non-TME^{Low} samples (Figure 2E). Interestingly, some of the most significantly downregulated genes (SLC2A5, CSF3R) were microglial-related. TME^{Med} was associated with several downregulated genes, including the B lymphocyte chemoattractant and TLS marker, CXCL13 compared to non-TME^{Med} samples (Figure 2F). Whereas TME^{High} GBM predominantly consisted of significantly upregulated genes including genes encoding for T-lymphocytes (CD6), surface antigens on T-cells (CD2) and cytokine CCL5 compared to non-TME^{High} samples (Figure 2G). Gene Ontology (GO) enrichment analysis in the GLITRAIN cohort revealed TME-subtype specific pathway alterations. TME^{Low} GBM was significantly enriched in pathways relating to EGFR signalling (P=0.02406)(Supplementary Figure 11A), and showed significantly downregulated immune-related pathways (Supplementary Figure 12A). TME^{Med} was enriched in pathways relating to neuronal signaling (Supplementary Figure 11B) and displayed downregulated immune-related pathways (Supplementary Figure 12B). TME^{High} GBM was significantly enriched in pathways relating to the immune system, including complement cascade and immunoregulatory interactions between lymphoid (P=2.4e-37) and non-lymphoid cells (P=7.9e-34)(Supplementary Figure 11C). In contrast, few significantly downregulated pathways were observed in TME^{High} (Supplementary Figure 12C).

To address spatial heterogeneity of TME subtype expression signatures, the IvyGAP dataset (*N*=122 samples) was stratified according to novel TME classifiers (Supplementary Figure 13A). Spatial interrogation of TME subtype distribution (based on IvyGAP anatomic neighbourhoods), identified differing gene expression patterns among each anatomic region. TME^{High} samples were most enriched within regions defined as cellular tumour (63%). TME^{High} samples also demonstrated slightly elevated proportions of microvascular proliferation samples (12%) compared to other subtypes. The TME^{Med} cohort manifested a moderate proportion of infiltrating tumour samples (10%) and elevated proportion of microvascular proliferation samples (15%) compared to TME^{Low} samples (6%). In contrast, TME^{Med} samples displayed the highest proportion of pseudopalisading cells around necrosis samples (23%). Finally, the TME^{Low} cohort contained the highest proportion of infiltrating tumour (14%) and leading edge (12%) samples. An additional subgroup (12.6%), which displayed an enriched expression of endothelial (*P*=<2.2e-16) and myeloid dendritic cells (p=3.5e-16), was further identified upon IvyGAP sample clustering (Cluster EC, Supplementary Figure 13). This cluster most frequently manifested with leading edge samples (20%) compared with TME^{Low}, TME^{Med} or TME^{High} subtypes (Supplementary Figure 13B).

Longitudinal analysis of TME-subtypes reveals TME-subtype 'switch' on recurrence

To assess TME-subtype evolution and identify changes in TME composition at tumour recurrence, we next analysed a set of longitudinal transcriptomic data from the GLASS longitudinal cohort (*N*=99 patients with primary and recurrent tumours)[17]. Firstly, TME-

subtypes were applied to primary and recurrent GLASS cohort tumours (*N*=367 tumour samples representing primary and recurrence 1-4), followed by assessment of functional orientation markers and immune checkpoint expression. These analyses revealed T cells, CD8 T cells, B lineage and PD1 expression were significantly enriched in recurrent tumours (Figure 3A). Next, we categorised the GLASS cohort according to novel TME-subtypes (Supplementary Figure 14A) identifying a higher proportion of TME^{Med} (39%) and TME^{High} (22%) cases in recurrent samples when compared to primary tumours (33% and 12% respectively)(Figure 3B,C). The proportion of TME^{Low} tumour s decreased from 55% to 39% upon recurrence. Tumours which transitioned from TME^{Low} to TME^{Med} upon recurrence, presented significantly elevated lymphocyte-associated gene expression. Specifically, T cells (*P*=5.4e-06), CD8 T cells (*P*=2.3e-10), cytotoxic lymphocytes (*P*=0.022) and B lineage (*P*=0.00085) expression markers were elevated (Figure 3D). TME^{Low} to TME^{High} transitions revealed significantly enriched lymphocytes and monocytic lineage (Figure 3E). TME^{Med} to TME^{High} subtype transition showed a significant enrichment across immune and stromal cell populations (excluding microglia)(Figure 3F). Unsurprisingly, tumours which switched to more immune cold subtypes displayed significantly decreased immune populations (Supplementary Figure 14B,C). In depth cell-state analysis revealed TME^{Med} to TME^{High} transition was influenced by a significantly enriched myeloid cell state *(P*=0.0019). Moreover, Stem-like and diff-like neoplastic states were significantly downregulated upon this transition (*P*=0.04 and *P*=0.00049 respectively)(Supplementary Figure 15A-C). DEG analysis revealed several significantly upregulated chemokine-signaling related pathways upon TME^{Med} to TME^{High} switch (Supplementary Figure 15D). Moreover, tumour promoting chemokines, CCL18 and

ACP5, were highly upregulated upon subtype switch (Supplementary Figure 15E). In a very limited number of available longitudinal GLASS cohort samples (*N*=4) from patients treated with immunotherapy, we assessed whether trends in TME subtype switch are altered following treatment (Supplementary Figure 14D). Unsurprisingly, findings were inconclusive, with transitions from TME^{Med} to TME^{Low} (*N*=1), TME^{Med} to TME^{High} (*N*=1) and TME^{Low} to TME^{Med} (*N*=2) observed.

TME-subtypes may inform treatment outcome in retrospective immunotherapy trial datasets

We subsequently examined whether patient stratification based on TME-subtype could predict response to immune checkpoint blockade. To this end, we accessed RNA-seq and clinical annotation data from the recent neoadjuvant anti-PD1 multi-institution clinical trial (Cloughesy cohort)[13]. This trial evaluated immune responses and survival following neoadjuvant and/or adjuvant therapy with pembrolizumab in patients with recurrent, surgically-resectable GBM. Firstly, IDHmt samples (*N*=4) were identified and excluded. Subsequently, TME classifiers were assigned to the trial cohort (Figure 4A). TME^{High} tumour-bearing patients displayed a trend towards improved OS when compared with TME^{Low} and TME^{Med} tumour-bearing patients (*P*=0.29)(Figure 4B). Importantly, TME^{High} patients treated with neoadjuvant anti-PD1 exhibited a significantly increased OS compared with neoadjuvant anti-PD1 treated non-TME^{High} (TME^{Low} and TME^{Med}) patients and TME^{Med} patients treated with adjuvant anti-PD1 (*P*=0.028)(Figure 4C,D).

Next, to further study the relationship between TME-subtype and response to ICI, we accessed RNA-seq data from the Zhao study (Zhao cohort) which evaluated immune responses and survival of longitudinally profiled patients during standard therapy and following treatment with PD-1 inhibitors (nivolumab or pembrolizumab)[18]. Firstly, the GBM-MCP-counter was applied to pre- and post-anti-PD1 treated tumour samples (n=24)(Figure 5A). Comparison of pre- and post-treatment samples revealed tumours receiving adjuvant anti-PD1 displayed no significantly different GBM-MCP scores. Next, samples were assigned to novel TME-subtypes. Survival analysis showed a trend towards improved OS in TME^{High} compared to non-TME^{High} patients (TME^{Low}/TME^{Med})(*P*=0.21)(Figure 5B). We subsequently assessed how TME-subtype proportion changes in pre- and post-anti-PD1 treatment samples, and in responders and non-responders (responders defined as those which revealed an inflammatory response, few tumour cells upon sampling and stable or shrinking tumour volume). Following anti-PD1 treatment, the proportion of TME^{Low} tumours remained the same (33%), the proportion of TME^{Med} tumours decreased from 27% to 22%, and the proportion of TME^{High} tumours increased from 40% to 44% (Figure 5C). Based on pre-treatment tumour samples, TME^{Low} proportion was greater in responders (7%) compared to non-responders (20%). Likewise, 43% of TME^{High} were responders compared with 40% non-responders. No TME^{Med} samples were categorised as responders (Supplementary Figure 16). Comparison of GBM-MCP scores in non-responders and responders, and in pre- and post- ICI treated (*N*=3) samples (Supplementary Figure 17) indicated no significant changes in TME populations.

Finally, we examined whether patient stratification based on TME-subtype could predict response to oncolytic virus therapy. Sequencing and clinical data were accessed from the Desjardins et al [19] 2018 phase 1 clinical trial (NCT01491893) which evaluated convection-enhanced, intratumoural delivery of recombinant non-pathogenic polio–rhinovirus chimera (PVSRIPO) in rGBM patients (PVSRIPO cohort). Samples were first assigned to TME-subtypes (Figure 5E). Tentatively, TME^{High} patients treated with PVSRIPO showed a trend towards improved OS (P=0.056) when compared with TME^{Low} and TME^{Med} tumours (Figure 5F).

Discussion

Notwithstanding the plausible rationale which has supported immune checkpoint inhibitor evaluation in GBM trials,[7,28] to date, clinical studies have largely been negative[9,10] with few exceptions[13,29,30]. Of these, [31,32]recent data from a small multi-centre trial (Cloughesy study) suggests that neoadjuvant nivolumab may improve OS compared to patients receiving adjuvant therapy[13]. Furthermore, mechanistic interrogation of the immunemicroenvironment following administration of neo-adjuvant nivolumab revealed increased immune cell infiltration, chemokine transcript expression and greater T-cell antigen receptor (TCR) diversity among TILs[29]. Notwithstanding these important, hypothesis generating data, most negative clinical trial outcomes[9–12] now mandate the identification of new stratification methods to identify a sub-population of patients for whom immunotherapy could be a viable option. To this end, we hypothesized that interrogation of the TME, including the identification of novel TME-associated subtypes might predict which patients would be

most responsive to immunotherapy and have generated robust hypotheses for novel subtype-specific combinatorial immunotherapy treatment regimens, which now warrant further testingspan style="font-family:Arial"> [2].

To identify novel TME specific classifiers, we implemented a tailored, brain tumour-specific MCP-counter[14] method. Specifically, unsupervised PAM clustering was applied to GBM-MCP-counter scores in discovery and validation cohorts (*N*=867 primary/recurrent patient samples) to identify three, non-overlapping TME-subtypes: TME^{Low}, TME^{Med}, and TME^{High}. Survival analysis revealed that there was no subtype-specific prognostic association. This is unsurprising as discovery and validation cohorts were normalized for KPS and age and included only IDHwt samples. Moreover, GBM-MCP-counter scores are based on genes which have no clear prognostic value when assessed as individual biomarkers[31]. We observed an overlap between novel TME-subtypes and Wang transcriptomic classifiers. However, we observed no survival differences following classification according to Wang-subtypes[21]. There was no significant difference in neoantigen load across TME classifiers, and a low tumour mutational burden was observed across all subtypes. Interestingly, Zhang et al have recently shown that methylated MGMT and low TIM3 expression are associated with improved survival in GBM[32]. However, in our analyses TIM3 expression was homogenous across subtypes. No significant relationship was observed between MGMT methylation status and novel TME subtype.

TME^{Low} GBM is associated with low immune and endothelial cell abundance, low expression of genes associated with TME functional orientation and overall downregulated immune-regulatory pathways TME^{Low} tumours also manifested the highest proportion of infiltrating tumour and leading-edge samples within the IvyGAP cohort compared to TME^{High} and TME^{Med} patient samples. Mutational and GO analysis showed that EGFR mutation and upregulated EGFR signaling pathways were dominant features of TME^{Low} GBM. As TME^{Low} patients exhibit overall low immune cell abundance, our data indicate that patients categorised as TME^{Low} may be the most suitable candidates for a prospective clinical trial evaluating the combination of anti-TIM3 combined with an EGFR inhibitor. This strategy would concurrently target the high EGFR mutational burden of TME^{Low} patients whilst stimulating T-cell infiltration. Recently, it has been suggested that EGFR therapeutic resistance may arise due to extrachromosomal DNA (ecDNA) amplification, rather than classical chromosomal alterations[33]. Further interrogation of TME^{Low} ecDNA landscape is required to uncover potential resistance mechanisms which may be hallmarks of this subtype.

TME^{Med} GBM is associated with an abundance of immune populations, functional orientation markers, immune checkpoint and endothelial cell markers. TME subtype analysis of IvyGAP anatomical samples revealed TME^{Med} patients comprised the highest proportion of samples defined as ‘pseudopalisading cells around necrosis’. Interestingly, pseudopalisades are associated with microvascular hyperplasia and angiogenesis, and may serve as predictors of poor prognosis in GBM[34]. Thus, despite negative outcomes following anti-angiogenic therapy (NCT00884741 and Checkmate-143/NCT02017717), our

data tentatively suggests that patients identified in the 'colder' TME^{Med} subtype might anti-angiogenic treatment combined with immunotherapy due to high endothelial cell abundance, vascularity and diverse immune cell population. Additionally, titin (TTN) mutation was identified as a TME^{Med} tumour feature. While TTN mutations are associated with favourable prognosis in non-small cell lung cancer[35], mutant TTN may be associated with increased risk of glioma recurrence[36] suggesting that TTN mutations could influence GBM TME^{Med} tumour recurrence. GO analysis of TME^{Med} tumours further revealed upregulated neuronal system-related and transmission across chemical synapses pathways. We and others have recently shown that increased GBM growth and invasion is facilitated by neuron-to-glioma synapses and increased neuronal interactions at recurrence[37,38]. Overall, future studies are now required to interrogate the role of TTN and neuronal-tumour interactions in TME^{Med} GBM recurrence and tumour progression.

TME^{High} tumours were defined by high immune cell infiltration and abundance of endothelial cells. Additionally, TME^{High} tumours are enriched for markers associated with T cell activation, MHC I genes, myeloid cell chemotaxis, inhibitory T cells, regulatory T cells, tumour associated macrophage and Immune checkpoints. These markers are indicative of a highly immunosuppressive, tumour-promoting environment[39,40]. Targeting specific cell populations to alleviate immunosuppression in TME^{High} GBM will likely be required to maximize response to immunotherapy. Interestingly, 65% of TME^{High} tumours were identified as Mes, suggesting that a subpopulation of Mes patients may respond to ICI, with TME subtyping representing a more refined predictive classification approach. TME subtype analysis of IvyGAP anatomical samples revealed TME^{High} patients comprised the

highest proportion of samples defined as 'microvascular proliferation' regions, a classical hallmark of GBM. DEGs and GO analysis in TME^{High} tumours further revealed several upregulated genes and pathways related to immunoregulation. Interestingly, TLSs (and an associated transcriptomic signature) were specifically identified in TME^{High}/mesenchymal+ tumours. TLSs have been associated with clinical benefit and response to immunotherapy in solid tumours[41], however the clinical relevance of TLSs in GBM remains unclear[42]. Our data suggests that monocytic lineage abundance may influence mechanisms which impact OS of TLS^{High} patients. The immunosuppressive role of TAMs[27,43] and their role in inducing a mesenchymal-like state in GBM[44] is well documented. Thus, in TME^{High} GBM, TAMs may suppress TLS anti-tumour activity, hindering immunotherapy response. Future studies to confirm the promiscuity of TLSs and associated subsets of immunosuppressive macrophages in TME^{High} tumours is warranted[45]. Overall, our data suggests that targeting anti-PD1+anti-CTLA4, may be a viable approach although it is noteworthy that a previous Phase 1 trial identified concerning treatment related adverse effects (AEs) in rGBM patients treated with combinatorial nivolumab and ipilimumab therapy, followed by nivolumab monotherapy, Specifically, grade 3/4 AEs were reported in 90% of patients who received 1mg/kg nivolumab plus 3mg/kg ipilimumab (NIVO1+IPI3), and 30% of patients who received 3mg/kg nivolumab plus 1mg/kg ipilimumab (NIVO3+IPI1)[11]. A rational alternative strategy in this sub-cohort could be anti-PD1+TAM targeting (e.g. CSFR1 inhibitor).

Longitudinal assessment of TME-subtypes has also revealed their dynamic nature. Tumours which transitioned from TME^{Low} to TME^{Med} or TME^{High}, and TME^{Med} to TME^{High}, were

associated with significantly enriched lymphocytes, myeloid population abundance, T-cell functionality and an immunosuppressive TME. Importantly, we and others have recently shown that IDHwt GBM recurrence may be attributed to increased immune cell composition, and presence of a myeloid cell state. Moreover, this enriched myeloid cell state is associated with a mesenchymal subtype shift [37]. Here we investigated whether TME subtypes are driven from a “lower to higher” TME status by changes in the neoplastic (Proliferative stem-like, Stem-like and Differentiated-like) and myeloid cell state upon recurrence[37]. Our data suggests that TME^{Med} to TME^{High} switch is influenced by a distinct myeloid phenotype, decreased tumour cell differentiation and upregulated chemokine-pathways. Moreover, CCL18 (promotes glioma progression) and ACP5 (mediator of glioma growth) were highly upregulated upon subtype switching.[46,47]. Overall, this pathway may harbour potential therapeutic avenues for the treatment of patients with tumours which transition from TME^{Med} to TME^{High} upon recurrence. To further understand subtype evolution and treatment resistance, scRNA-seq analysis and construction of dynamic cellular models to inform TME plasticity, cellular lineage and trajectory, is now required. It will also be important to consider whether therapeutic pressure may truly drive subtype switching[41,48]. Additional analyses of biopsies in primary and recurrent tumours (post-treatment) may further unravel the impact of intra-tumoural heterogeneity on TME-subtype classification and TME-subtype specific treatment resistance mechanisms[37].

Finally, the predictive potential of novel TME-subtypes was retrospectively assessed in interventional immunotherapy clinical trial datasets. Firstly, our analysis of the small Cloughesy trial dataset tentatively suggests that TME^{High} patients who receive neoadjuvant

anti-PD1 might show improved OS compared to patients receiving adjuvant anti-PD1 alone. Nevertheless, we acknowledge that TME stratification prior to neoadjuvant treatment is not without complexity. However, we hypothesize that in the future, TME subtyping might be performed prior to surgery by employing a blood based cell free RNA (cfRNA) liquid biopsy method[49], or a robust TME subtype specific MRI radiomic signature[50,51]. Secondly, analysis of the Zhao cohort suggests that TME^{High} tumour-bearing patients trend towards improved OS following anti-PD1 therapy. In a very limited subset of matched samples collected pre- and post- ICI therapy (*N*=3 patients), no significant alterations were detected in MCP scores before or after treatment (Supplementary Figure 17). As mentioned above, conclusions with respect to subtype switching may not be drawn from such a limited number of samples. Thus, further studies in expanded patient cohorts are now warranted. Interestingly, a relationship between TME subtype assigned at time of primary tumour resection and response to anti-PD1 was observed regardless of standard of care treatment regimen prior to anti-PD1 therapy. This observation also requires further validation. Thirdly, we investigated whether TME-subtypes were predictive of survival within the small PSVRIPO dataset (NCT01491893). Here, GBM patients received adjuvant anti-PD1 (newly diagnosed) or PVSRIPO therapy (recurrent tumours, treatment administered post biopsy). Stratification of PVSRIPO patients based on TME-subtypes suggest a trend towards improved OS in TME^{High} patients, compared with TME^{Med} and TME^{Low} patients. Clearly- hypotheses generating data now require validation in larger clinical cohorts. Desjardins have recently shown that a low mutational burden was associated with increased tumor-intrinsic inflammation in rGBM and increased response to PVSRIPO treatment[52]. Interestingly, our data suggests that TME^{High}

patients may harbour a lower mutational burden than other subtypes, yet represent the subtype with the highest proportion of ICI responders.

Overall as mentioned, while we observe promising trends in all trial cohorts assessed, sample numbers are limited. Moreover, each trial cohort analysed has a unique study design and implements a specific immunotherapy regimen. Furthermore, an important study limitation is that validation of our findings in an expanded cohort of samples from recently conducted negative Phase III trials (e.g. Checkmate-143, Checkmate-548 and Checkmate-498) has not been possible due to lack of availability of tissue/ RNAseq data. A tailored, Phase 2 study employing a rational hypothesis- driven trial design is now required to validate our findings. This trial should mandate for the robust collection of fresh frozen tissue for retrospective molecular analysis.

In conclusion, our multi-centre study introduces novel TME-subtypes which may inform optimal precision immunotherapy treatment strategies in the GBM setting. Our data provides convincing evidence that a TME-subtype classification system represents a canonical "*terminus a quo*" (starting point) to (i) deepen knowledge of GBM TME biology, (ii) support identification of patient subgroups who may benefit from immunotherapy and/or other TME targeting agents and (iii) provide a platform for the identification of new TME-associated contexts of vulnerability. Our findings warrant further investigation in additional retrospective immunotherapy trial cohorts, and in the prospective setting.

Acknowledgements

The work presented in this paper is dedicated to the memory of Mr Paolo Iacovelli. We would like to thank J. Heffernan, L.M Houlihan and J. Mythen (Beaumont Hospital Neuropathology Dept) for their help in establishing the GLIOTRAIN biobank in Dublin. The authors gratefully acknowledge all patients who kindly donated tumour tissue and clinical/ genomic data used in this study.

Funding information

This project has received funding from the European Union's Horizon 2020 research and innovation programme under the Marie Skłodowska-Curie ITN initiative (Grant Agreement #766069, GLIOTRAIN (http://www.gliotrain.eu) and 'GLIORESOLVE' projects (Grant Agreement #101073386). Additional support was received by donation from the Paolo Iacovelli memorial endowment. We are also grateful for financial support from the Beaumont Hospital Foundation, and from Brain Tumour Ireland to establish the Beaumont Hospital Brain Tumour Biorepository. The authors further acknowledge financial contribution towards staff salaries from RCSI and Champions Oncology (Baltimore, US).

Disclosure

The authors declare no conflict of interest. The funders had no role in the design of the study; in the collection, analyses, or interpretation of data; in the writing of the manuscript, or in the decision to publish the results.

Bibliography

1. Brat DJ, Aldape K, Colman H, Figrarella-Branger D, Fuller GN, Giannini C, et al. cIMPACT-NOW update 5: recommended grading criteria and terminologies for IDH-mutant astrocytomas. *Acta Neuropathol*. March 1, 2020;139(3):603–608.
2. White K, Connor K, Clerkin J, Murphy BM, Salvucci M, O'Farrell AC, et al. New hints towards a precision medicine strategy for IDH wild-type glioblastoma. *Annals of Oncology*. September 2020;
3. Schiffer D, Annovazzi L, Casalone C, Corona C, Mellai M. Glioblastoma: Microenvironment and niche concept. Vol. 11, Cancers. MDPI AG 2019.
4. Berghoff AS, Kiesel B, Widhalm G, Rajky O, Ricken G, Wöhrer A, et al. Programmed death ligand 1 expression and tumor-infiltrating lymphocytes in glioblastoma. *Neuro Oncol*. August 2015 [cited November 29, 2017];17(8):1064–1075. Available at: http://www.ncbi.nlm.nih.gov/pubmed/25355681
5. Nduom EK, Wei J, Yaghi NK, Huang N, Kong L-Y, Gabrusiewicz K, et al. PD-L1 expression and prognostic impact in glioblastoma. *Neuro Oncol*. February 2016 [cited November 29, 2017];18(2):195–205. Available at: http://www.ncbi.nlm.nih.gov/pubmed/26323609
6. Preusser M, Lim M, Hafler DA, Reardon DA, Sampson JH. Prospects of immune checkpoint modulators in the treatment of glioblastoma. *Nat Rev Neurol*. September 11, 2015;11(9):504–514. Available at: http://www.nature.com/articles/nrneurol.2015.139
7. Reardon DA, Gokhale PC, Klein SR, Ligon KL, Rodig SJ, Ramkissoon SH, et al. Glioblastoma Eradication Following Immune Checkpoint Blockade in an Orthotopic, Immunocompetent Model. *Cancer Immunol Res*. February 1, 2016 [cited November 29, 2017];4(2):124–135. Available at: http://www.ncbi.nlm.nih.gov/pubmed/26546453
8. Yuan B, Wang G, Tang X, Tong A, Zhou L. Immunotherapy of glioblastoma: recent advances and future prospects. *Hum Vaccin Immunother*. March 28, 2022;1–16.
9. Reardon DA, Brandes AA, Omuro A, Mulholland P, Lim M, Wick A, et al. Effect of Nivolumab vs Bevacizumab in Patients with Recurrent Glioblastoma: The CheckMate 143 Phase 3 Randomized Clinical Trial. *JAMA Oncol*. 2020;6(7):1003–1010.
10. Bristol Myers Squibb. Bristol Myers Squibb: Checkmate-548 [Internet]. 2019 [cited April 21, 2022]. Available at: https://tinyurl.com/j6v2zkkj
11. Omuro A, Vlahovic G, Lim M, Sahebjam S, Baehring J, Cloughesy T, et al. Nivolumab with or without ipilimumab in patients with recurrent glioblastoma: Results from exploratory phase i cohorts of CheckMate 143. *Neuro Oncol*. 2018;20(5):674–686.
12. Bristol-Myers Squibb. Bristol-Myers Squibb Announces Phase 3 CheckMate -498 Study Did Not Meet Primary Endpoint of Overall Survival with Opdivo (nivolumab) Plus Radiation in Patients with Newly Diagnosed MGMT-Unmethylated Glioblastoma Multiforme. 2019 [cited May 4, 2022]; Available at: https://news.bms.com/news/corporate-financial/2019/Bristol-Myers-Squibb-Announces-Phase-3-CheckMate--498-Study-Did-Not-Meet-Primary-Endpoint-of-Overall-Survival-with-Opdivo-nivolumab-Plus-Radiation-in-Patients-with-Newly-Diagnosed-MGMT-Unmethylated-Glioblastoma-Multiforme/default.aspx

13. Cloughesy TF, Mochizuki AY, Orpilla JR, Hugo W, Lee AH, Davidson TB, et al. Neoadjuvant anti-PD-1 immunotherapy promotes a survival benefit with intratumoral and systemic immune responses in recurrent glioblastoma. *Nat Med*. March 11, 2019;25(3):477–486. Available at: http://www.nature.com/articles/s41591-018-0337-7
14. Becht E, Giraldo NA, Lacroix L, Buttard B, Elarouci N, Petitprez F, et al. Estimating the population abundance of tissue-infiltrating immune and stromal cell populations using gene expression. *Genome Biol*. December 20, 2016 [cited March 25, 2019];17(1):218. Available at: http://genomebiology.biomedcentral.com/articles/10.1186/s13059-016-1070-5
15. McLendon R, Friedman A, Bigner D, van Meir EG, Brat DJ, Mastrogianakis GM, et al. Comprehensive genomic characterization defines human glioblastoma genes and core pathways. *Nature*. October 23, 2008;455(7216):1061–1068. Available at: http://www.nature.com/articles/nature07385
16. Zhao Z, Zhang KN, Wang Q, Li G, Zeng F, Zhang Y, et al. Chinese Glioma Genome Atlas (CGGA): A Comprehensive Resource with Functional Genomic Data from Chinese Glioma Patients. *Genomics Proteomics Bioinformatics*. February 1, 2021;19(1):1–12.
17. Aldape K, Amin SB, Ashley DM, Barnholtz-Sloan JS, Bates AJ, Beroukhim R, et al. Glioma through the looking GLASS: Molecular evolution of diffuse gliomas and the Glioma Longitudinal Analysis Consortium. *Neuro Oncol*. 2018;20(7):873–884.
18. Zhao J, Chen AX, Gartrell RD, Silverman AM, Aparicio L, Chu T, et al. Immune and genomic correlates of response to anti-PD-1 immunotherapy in glioblastoma. *Nat Med*. March 11, 2019;25(3):462–469. Available at: http://www.nature.com/articles/s41591-019-0349-y
19. Desjardins A, Gromeier M, Herndon JE, Beaubier N, Bolognesi DP, Friedman AH, et al. Recurrent Glioblastoma Treated with Recombinant Poliovirus. *New England Journal of Medicine*. July 12, 2018;379(2):150–161.
20. Klemm F, Maas RR, Bowman RL, Kornete M, Soukup K, Nassiri S, et al. Interrogation of the Microenvironmental Landscape in Brain Tumors Reveals Disease-Specific Alterations of Immune Cells. *Cell*. 2020;181(7):1643-1660.e17. Available at: https://doi.org/10.1016/j.cell.2020.05.007
21. Wang Q, Hu B, Hu X, Kim H, Squatrito M, Scarpace L, et al. Tumor Evolution of Glioma-Intrinsic Gene Expression Subtypes Associates with Immunological Changes in the Microenvironment. *Cancer Cell*. July 2017;32(1):42-56.e6.
22. Nehama D, di Ianni N, Musio S, Du H, Patané M, Pollo B, et al. B7-H3-redirected chimeric antigen receptor T cells target glioblastoma and neurospheres. *EBioMedicine*. September 1, 2019;47:33–43.
23. Zhang J, Wang J, Marzese DM, Wang X, Yang Z, Li C, et al. B7H3 regulates differentiation and serves as a potential biomarker and theranostic target for human glioblastoma. *Laboratory Investigation*. July 1, 2019;99(8):1117–1129.
24. Zhang C, Zhang Z, Li F, Shen Z, Qiao Y, Li L, et al. Large-scale analysis reveals the specific clinical and immune features of B7-H3 in glioma. *Oncoimmunology*. November 2, 2018;7(11).

25. Digregorio M, Coppieters N, Lombard A, Lumapat PN, Scholtes F, Rogister B. The expression of B7-H3 isoforms in newly diagnosed glioblastoma and recurrence and their functional role. *Acta Neuropathol Commun*<="" span="">
26. Coppola D, Nebozhyn M, Khalil F, Dai H, Yeatman T, Loboda A, et al. Unique ectopic lymph node-like structures present in human primary colorectal carcinoma are identified by immune gene array profiling. *American Journal of Pathology*. July 2011;179(1):37–45.
27. Sautès-Fridman C, Petitprez F, Calderaro J, Fridman WH. Tertiary lymphoid structures in the era of cancer immunotherapy. Vol. 19, Nature Reviews Cancer. Nature Publishing Group 2019; 307–325.
28. Preusser M, Lim M, Hafler DA, Reardon DA, Sampson JH. Prospects of immune checkpoint modulators in the treatment of glioblastoma. *Nat Rev Neurol*. 2015;11(9):504–514.
29. Schalper KA, Rodriguez-Ruiz ME, Diez-Valle R, López-Janeiro A, Porciuncula A, Idoate MA, et al. Neoadjuvant nivolumab modifies the tumor immune microenvironment in resectable glioblastoma. *Nat Med*. 2019;25(3):470–476.
30. Lee AH, Sun L, Mochizuki AY, Reynoso JG, Orpilla J, Chow F, et al. Neoadjuvant PD-1 blockade induces T cell and cDC1 activation but fails to overcome the immunosuppressive tumor associated macrophages in recurrent glioblastoma. *Nat Commun*. December 1, 2021;12(1).
31. Kan LK, Drummond K, Hunn M, Williams D, O'Brien TJ, Monif M. Potential biomarkers and challenges in glioma diagnosis, therapy and prognosis. Vol. 2, BMJ Neurology Open. BMJ Publishing Group 2020.
32. Zhang J, Sai K, Wang X li, Ye S quan, Liang L jiao, Zhou Y, et al. Tim-3 Expression and MGMT Methylation Status Association With Survival in Glioblastoma. *Front Pharmacol*. September 15, 2020;11.
33. Nathanson DA, Gini B, Mottahedeh J, Visnyei K, Koga T, Gomez G, et al. Targeted therapy resistance mediated by dynamic regulation of extrachromosomal mutant EGFR DNA. *Science (1979)*. 2014;343(6166):72–76.
34. Brat DJ, van Meir EG. Vaso-occlusive and prothrombotic mechanisms associated with tumor hypoxia, necrosis, and accelerated growth in glioblastoma. Vol. 84, Laboratory Investigation. 2004; 397–405.
35. Cheng X, Yin H, Fu J, Chen C, An J, Guan J, et al. Aggregate analysis based on TCGA: TTN missense mutation correlates with favorable prognosis in lung squamous cell carcinoma. *J Cancer Res Clin Oncol*. April 2, 2019;145(4):1027–1035.
36. Wu P, Yang W, Ma J, Zhang J, Liao M, Xu L, et al. Mutant-allele tumor heterogeneity in malignant glioma effectively predicts neoplastic recurrence. *Oncol Lett*. 2019;18(6):6108–6116.
37. Varn FS, Johnson KC, Martinek J, Huse JT, Nasrallah MP, Wesseling P, et al. Glioma progression is shaped by genetic evolution and microenvironment interactions. *Cell*. June 1, 2022;185(12):2184-2199.e16. Available at: https://linkinghub.elsevier.com/retrieve/pii/S0092867422005360
38. Johnson KC, Anderson KJ, Courtois ET, Gujar AD, Barthel FP, Varn FS, et al. Single-cell multimodal glioma analyses identify epigenetic regulators of cellular

plasticity and environmental stress response. *Nat Genet*. October 1, 2021;53(10):1456–1468.
39. Togashi Y, Shitara K, Nishikawa H. Regulatory T cells in cancer immunosuppression — implications for anticancer therapy. *Nat Rev Clin Oncol*. Available at: https://doi.org/10.1038/s41571-
40. Takenaka MC, Gabriely G, Rothhammer V, Mascanfroni ID, Wheeler MA, Chao CC, et al. Control of tumor-associated macrophages and T cells in glioblastoma via AHR and CD39. *Nat Neurosci*. May 1, 2019;22(5):729–740.
41. Neftel C, Laffy J, Filbin MG, Hara T, Shore ME, Rahme GJ, et al. An Integrative Model of Cellular States, Plasticity, and Genetics for Glioblastoma. *Cell*. 2019;178(4):835-849.e21.
42. van de Walle T, Vaccaro A, Ramachandran M, Pietilä I, Essand M, Dimberg A. Tertiary Lymphoid Structures in the Central Nervous System: Implications for Glioblastoma. Vol. 12, Frontiers in Immunology. Frontiers Media S.A. 2021.
43. Petitprez F, Lévy S, Sun CM, Meylan M, Linhard C, Becht E, et al. The murine Microenvironment Cell Population counter method to estimate abundance of tissue-infiltrating immune and stromal cell populations in murine samples using gene expression. *bioRxiv*. 2020;
44. Hara T, Chanoch-Myers R, Mathewson ND, Myskiw C, Atta L, Bussema L, et al. Interactions between cancer cells and immune cells drive transitions to mesenchymal-like states in glioblastoma. *Cancer Cell*. June 2021;39(6):779-792.e11. Available at: https://linkinghub.elsevier.com/retrieve/pii/S1535610821002683
45. Goswami S, Walle T, Cornish AE, Basu S, Anandhan S, Fernandez I, et al. Immune profiling of human tumors identifies CD73 as a combinatorial target in glioblastoma. Vol. 26, Nature Medicine. Nature Research 2020; 39–46.
46. Huang Y, Motta E, Nanvuma C, Kuhrt LD, Yuan Y, Xia P, et al. Microglia/macrophage-derived human CCL18 promotes glioma progression via CCR8-ACP5 axis analyzed in humanized slice model. *Cell Rep*. April 12, 2022;39(2).
47. Grochans S, Korbecki J, Simińska D, Żwierełło W, Żeszotek S, Kolasa A, et al. CCL18 Expression Is Higher in a Glioblastoma Multiforme Tumor than in the Peritumoral Area and Causes the Migration of Tumor Cells Sensitized by Hypoxia. *Int J Mol Sci*. August 1, 2022;23(15).
48. Chaligne R, Gaiti F, Silverbush D, Schiffman JS, Weisman HR, Kluegel L, et al. Epigenetic encoding, heritability and plasticity of glioma transcriptional cell states. *Nat Genet*. October 1, 2021;53(10):1469–1479.
49. Müller Bark J, Kulasinghe A, Chua B, Day BW, Punyadeera C. Circulating biomarkers in patients with glioblastoma. Vol. 122, British Journal of Cancer. Springer Nature 2020; 295–305.
50. Zhang Z, He K, Wang Z, Zhang Y, Wu D, Zeng L, et al. Multiparametric MRI Radiomics for the Early Prediction of Response to Chemoradiotherapy in Patients With Postoperative Residual Gliomas: An Initial Study. *Front Oncol*. November 18, 2021;11.

51. Park JE, Kim HS, Jo Y, Yoo RE, Choi SH, Nam SJ, et al. Radiomics prognostication model in glioblastoma using diffusion- and perfusion-weighted MRI. *Sci Rep*. December 1, 2020;10(1).
52. Gromeier M, Brown MC, Zhang G, Lin X, Chen Y, Wei Z, et al. Very low mutation burden is a feature of inflamed recurrent glioblastomas responsive to cancer immunotherapy. *Nat Commun*. December 2021;12(1):1–7.

Figure Legends

Figure 1. Identification and validation of novel TME subtypes in GLIOTRAIN cohort and validation datasets (TCGA, CGGA, DUKE). A. Partition around medoids (PAM) clustering of the GLIOTRAIN cohort (N=123), based on the cellular TME composition described by MCP-counter scores reveals 3 subgroups; TMElow, TMEmed and TMEhigh in the B. TCGA, C. CCGA and D. DUKE cohorts E. OS according to TMElow, TMEmed and TMEhigh subtypes in the GLIOTRAIN cohort (P=0.55), F. TCGA cohort (P=0.53), G. CGGA cohort (P=0.13) and H. Duke cohort (P=0.55). I. Proportion of Wang subtypes22 in the TME classifiers. Statistical test A-D: Kruskal Wallis one-way analysis of variance. E-H: P value of log-ranked test. CL: Classical, Mes: Mesenchymal, PN: Proneural.

Figure 2. Characterisation of TME subtype specific biology. A. TME functional orientation markers and immune checkpoint expression across TME subtypes in the GLIOTRAIN discovery cohort. B. Neoantigen prediction across the TME subtypes in the TCGA cohort C. Mutation frequency across the TME subtypes in the TCGA cohort. D. TME subtype-specific mutation frequency for the top 10 genes with highest frequency in the TCGA cohort. E. Volcano plots showing differentially expressed genes in TME^{Low}, F. TME^{Med} and G. TME^{High} patients. Statistical test B,C: Kruskal Wallis one-way analysis of variance.

Figure 3. GBM TME and associated TME subtypes exhibit cellular heterogeneity upon recurrence. A. Heatmap showing the expression of GBM-MCP scores, FO markers and immune checkpoints in Primary tumours (TP), first recurrence (R1) and combined second, third and fourth recurrence in the GLASS cohort. B. Continuous bar graph showing the distribution of TME subtypes in matching primary and recurrent tumours (*N*=99 tumour pairs). C. Sankey plot indicating the transition of TME subtypes on recurrence. Band size reflects sample numbers and band colours represent TME subtype. D. Boxplots showing the TME cell populations with significantly enriched MCP-scores from primary to recurrent samples in patients who switch subtype; D. TME^{Low} (primary) to TME^{Med} (recurrent) tumours, E. TME^{Low} (primary) to $TMEHi^{gh}$ (recurrent) tumours and F. TME^{Med} (primary) to TME^{High} (recurrent) tumours. Statistical test: Wilcoxon signed rank test. * P<0.05 ***P<0.001

Figure 4. Trend towards improved OS following neoadjuvant pembrolizumab in recurrent IDHwt GBM TMEhigh patients. A. Partition around medoids (PAM) clustering of IDHwt GBM samples in the Cloughesy cohort13 with available RNA-seq data (*N*=23), based on the cellular TME composition described by GBM-MCP-counter scores reveal 3 subtypes; TME^{Low}, TME^{Med} and TME^{High}. B. OS according to TME^{Low}, TME^{Med} and TME^{High} subtypes in the Cloughesy cohort C. OS according to TMELow/neoadjuvant anti-PD-1, TMEMed/adjuvant anti-PD-1, TMEHigh/adjuvant anti-PD-1 and TMEHigh/adjuvant patients in the Cloughesy cohort. TMEMed patients treated with neoadjuvant anti-PD1 (*N*=1) and TME^{Low} patients treated with adjuvant anti-PD1 (*N*=2) were excluded due to small patient numbers D. Boxplot representing OS of patients in the Cloughesy cohort. Boxplots are colour coded according to the patients TME subtype and whether they received Neoadjuvant + adjuvant (Neo) anti-PD1 therapy or adjuvant (Adj) anti-PD1 alone. Orange; $TME^{High/Adj}$, Gold; $TME^{High/Neo}$, Green; $TME^{Low/Adj}$, Light blue; $TME^{Low/Neo}$, Dark blue;

TME$^{Med/Adj}$ and pink; TME$^{Med/Neo}$. Statistical test: Kaplan Meier analysis; P value of log-ranked test.

Figure 5. Trend towards improved OS and increased response rate in TME^{High} patients following adjuvant treatment with pembrolizumab or PVSRIPO . A. TME composition in Zhao dataset[18] pre- vs post- adjuvant anti-PD1 treatment in available tumour (*N*=24) samples. B. OS according to TME^{High} and non-TME^{High} (TME^{Low} + TME^{Med}) subtypes who received adjuvant anti-PD1 therapy in the Zhao cohort (*N*=15 patients). C. Relative boxplots indicating the proportion of TME^{Low,} TME^{Med} and TME^{High} patients before administration of anti-PD1 treatment (left) and after anti-PD1 treatment (right) in available tumour and blood samples. D. Partition around medoids (PAM) clustering of the PVSRIPO cohort[19] with available RNA-seq data (*N*=12), based on the cellular TME composition described by GBM-MCP-counter scores reveal 3 subtypes; TME^{low}, TME ^{med} and TME ^{high}. E. OS according to TME^{Low} and TME^{Med} and TME^{High} subtypes who received PVSRIPO therapy in the PVSRIPO cohort[19]. Statistical test: Wilcoxon signed rank test. Kaplan Meier analysis; P value of log-ranked test. **P*<0.05 ** *P*<0.01

Supplementary Figure 1. GBM dataset filtering process for the GLIOTRAIN cohort (discovery), TCGA, CGGA, and Duke cohorts (validation), the GLASS longitudinal cohort, IvyGAP cohort, Cloughesy, Zhao and PVSRIPO cohorts (Immunotherapy clinical trial cohorts).

Supplementary Figure 2. Refinement and immunohistochemical validation of MCP-counter for application in GBM. A. Representative images of the IHC and IF panel employed for MCP validation and authentication of GBM specific microglial signature. B. Correlation of GBM-MCP-counter scores with corresponding cell densities measured by IHC. Statistical analysis B: Spearman's rank correlation coefficient

Supplementary figure 3. Confirmation of novel TME subtypes as three distinct non-overlapping biological entities**. A.** Principle component analysis clustering of the TME^{Low}, TME^{Med} and TME^{High} subtypes in the GLIOTRAIN, **B.** TCGA, **C.** CGGA and **D.** DUKE cohorts.

Supplementary figure 4. Comparison of novel TME subtypes GBM-MCP scores in the **A.** GLIOTRAIN, **B.** TCGA **C.** CGGA and **D.** DUKE cohorts

Supplementary figure 5. Comparison of novel TME subtypes GBM-MCP scores in the A. GLIOTRAIN, B. TCGA C. CGGA and D. DUKE cohorts

Supplementary Figure 6. Immunohistochemical validation of TME subtypes. A. Partition around medoids (PAM) clustering of GLIOTRAIN "IHC sub-cohort" (*N*=26). GBM-MCP-counter scores ascribes this validation cohort to TME $^{low, med,high}$ subtypes. B. Subtypes were further validated via IHC staining. Representative images demonstrating CD3/CD20, CD8/CD66b, CD68 and SMA/PD-L1/CD34 expression by IHC of TME $^{low, med, high}$ tumours. **C.** Cell density counts showing the differences in immune and stromal composition across TME subtypes. Scale bar: 100um. Statistical test C: Kruskal Wallis one-way analysis of variance.

Supplementary Figure 7. Survival analysis across Wang subtypes (PN, CL and Mes), in the A. GLIOTRAIN cohort, B. TCGA cohort and C. CGGA cohort. Statistical test A-C: Kaplan Meier analysis; P value of log-ranked test.

Supplementary Figure 8. Characterisation of TME subtype specific biology in validation cohorts. A. Functional orientation and immune checkpoint expression of the TME sub-groups in the A. TCGA cohort, B. CGGA cohort and C. DUKE cohort.

Supplementary Figure 9. Tertiary Lymphoid structures (TLSs) and the 12-chemokine TLS signature may be a feature of TME^{High} GBM A. TLS aggregates are observed in TME^{High} tumours (*N*=3) in the GLIOTRAIN "IHC sub-cohort" via IHC (CD20/CD3). B. Heat map demonstrating expression of T cells, CD8 T cells, B lineage, NK cells and TLS-associated 12-chemokine signature across subtypes. C. Assessment of survival in GLIOTRAIN cohort (*N*=123) based on TLS signature expression. No significant different is observed in OS of GBM patients according to TLS signature expression (*P*=0.095). TLS High and low subgroups were calculated based on median threshold of TLS signature. D. Assessment of survival in GLIOTRAIN cohort (*N*=123) based on TLS and monocytic lineage signature expression. OS of patients based on the TLS-signature and monocytic lineage abundance. Tumours were classified as TLS signature High and monocytic lineage High based on median threshold**.** Monocytic $lineage^{High}/TLS^{Low}$ GBMs display a trend towards poorer OS (*P*=0.011). **E.** Gene expression heatmap of antigen-presenting cell (APC) and T cell activating and inhibitory signalling mediators in TLS^{Low} and TLS^{High} subgroups in GLIOTRAIN cohort (*N*=123). Scale bars: 500um. Statistical test C,D: Kaplan Meier analysis; P value of log-ranked test.

Supplementary figure 10. Comparison of MGMT methylation status across the TME subtypes in A. GLIOTRAIN, B. TCGA, C. CGGA and D. Duke cohorts

Supplementary Figure 11. Gene Ontology (GO) analysis in TME^{Low}, TME^{Med} and TME^{High} subtypes (GLIOTRAIN cohort). GO analysis showing the 10 most upregulated pathways (Bioplanet 2019) in A. TME^{Low}, B. TME^{Med} and C. TME^{High} subtypes.

Supplementary Figure 12. Gene Ontology (GO) analysis in TME^{Low}, TME^{Med} and TME^{High} subtypes (GLIOTRAIN cohort). GO analysis showing the 10 most downregulated pathways (Bioplanet 2019) in A. TME^{Low}, B. TME^{Med} and C. TME^{High} subtypes.

Supplementary Figure 13. Histological features correlate to TME subtype distribution. A. Partition around medoids (PAM) clustering of the Ivy GAP GBM cohort (n=10 patients), based on the cellular TME composition described by MCP-counter scores reveal 3 subgroups; TME low, TME med and TME high in the Ivy GAP cohort. B. Distribution of TME subtypes based on Ivy GAP histological features.

Supplementary Figure 14. Longitudinal analysis of TME subtypes and TME composition upon recurrence (GLASS cohort). Heatmap of GBM-MCP cell distribution in primary and recurrent IDHwt GBM samples from the GLASS cohort ([17] n=99 tumour pairs). B.

Boxplots showing significant changes in GBM-MCP score when samples 'switch' from B. TME^{Med} to TME^{Low} and C. TME^{High} to TME^{Med} upon recurrence. D. Sankey plot indicating the transition of TME subtypes on recurrence based on immunotherapy treatment. Band size reflects sample numbers and band colours represent TME subtype. Statistical test: Wilcoxon signed rank test.

Supplementary Figure 15. Cell-state changes and upregulated chemokine pathways are associated with TME subtype transitions upon recurrence. A. Boxplots showing the non-neoplastic cell-states (Myeloid) and neoplastic cell-states (Prolif stem-like, Stem-like and Diff-like) from primary to recurrent samples in patients who switch subtype; TME^{Low} (primary) to TME^{Med} (recurrent) tumours, B. TME^{Low} (primary) to TME^{High} (recurrent) tumours and C. TME^{Med} (primary) to TME^{High} (recurrent) tumours. D. GO analysis showing the 10 most upregulated pathways (Bioplanet 2019) in samples which transitioned from TME^{Med} to TME^{High} upon recurrence. E. Volcano plots showing differentially expressed genes in samples which transitioned from TME^{Med} to TME^{High} upon recurrence. Statistical test: Wilcoxon signed rank test.

Supplementary Figure 16. Comparison of GBM-MCP scores and TME subtype distribution in non-responders and responders in the Zhao cohort A. GBM-MCP scores categorized based on non-responders and responders in the Zhao cohort. B Relative bargraph indicating the proportion of $TME^{Low,}$ TME^{Med} and TME^{High} patients who are classified as Non-responders (left) and responders (right) according to Zhao et al., in available tumour samples.

Supplementary Figure 17. Comparison of TME composition in patients with matched pre- and post anti-PD1 treated samples. A. MCP scores categorized based on patients with matched Pre anti-PD1 treated and post-anti-PD1 treated samples in the Zhao cohort (*N*=3).

‡Annex I

GLIOTRAIN Consortium

- Martine Lamfers - m.lamfers@erasmusmc.nl
- Sieger Leenstra - s.leenstra@erasmusmc.nl
- Ioannis Ntafoulis - i.ntafoulis@erasmusmc.nl
- Federica Fabro - f.fabro@erasmusmc.nl
- JM Kros - j.m.kros@erasmusmc.nl

- Emie Quissac - Emie.quissac@icm-institute.org
- Archita Biswas - architabiswas@rcsi.ie
- J Cryan - janecryan@beaumont.ie
- F Brett - francescabrett@beaumont.ie
- A Beausang - alanbeausang@beaumont.ie
- S MacNally - stephenmacnally@beaumont.ie
- Phil O'Halloran - philohalloran@rcsi.ie
- James Clerkin - jamesclerkin@rcsi.ie
- Orna Bacon - ornabacon@gmail.com
- Diether Lambrechts - diether.lambrechts@kuleuven.be
- Gonca Dilcan - gonca.dilcandurdag@kuleuven.be
- Francesca Lodi - francesca.lodi@kuleuven.be
- Ingrid Arijs - ingrid.arijs@kuleuven.be
- Andreas Kremer - andreas.kremer@ittm-solutions.com
- Romain Tching Chi Yen - romain.tching@ittm-solutions.com

1

[1] Referred to throughout as “GBM” based on recent c-IMPACT-NOW[1] recommendations

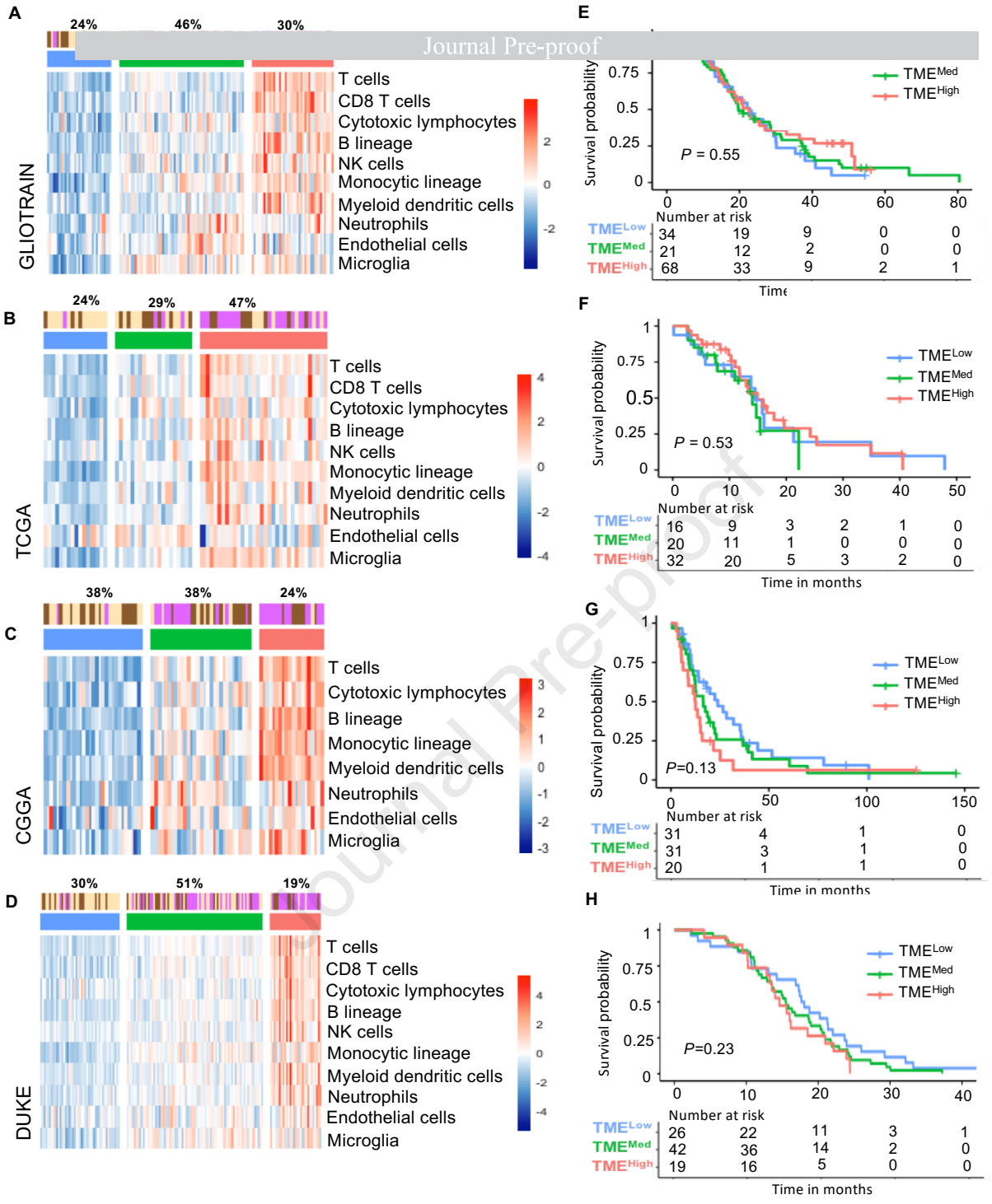

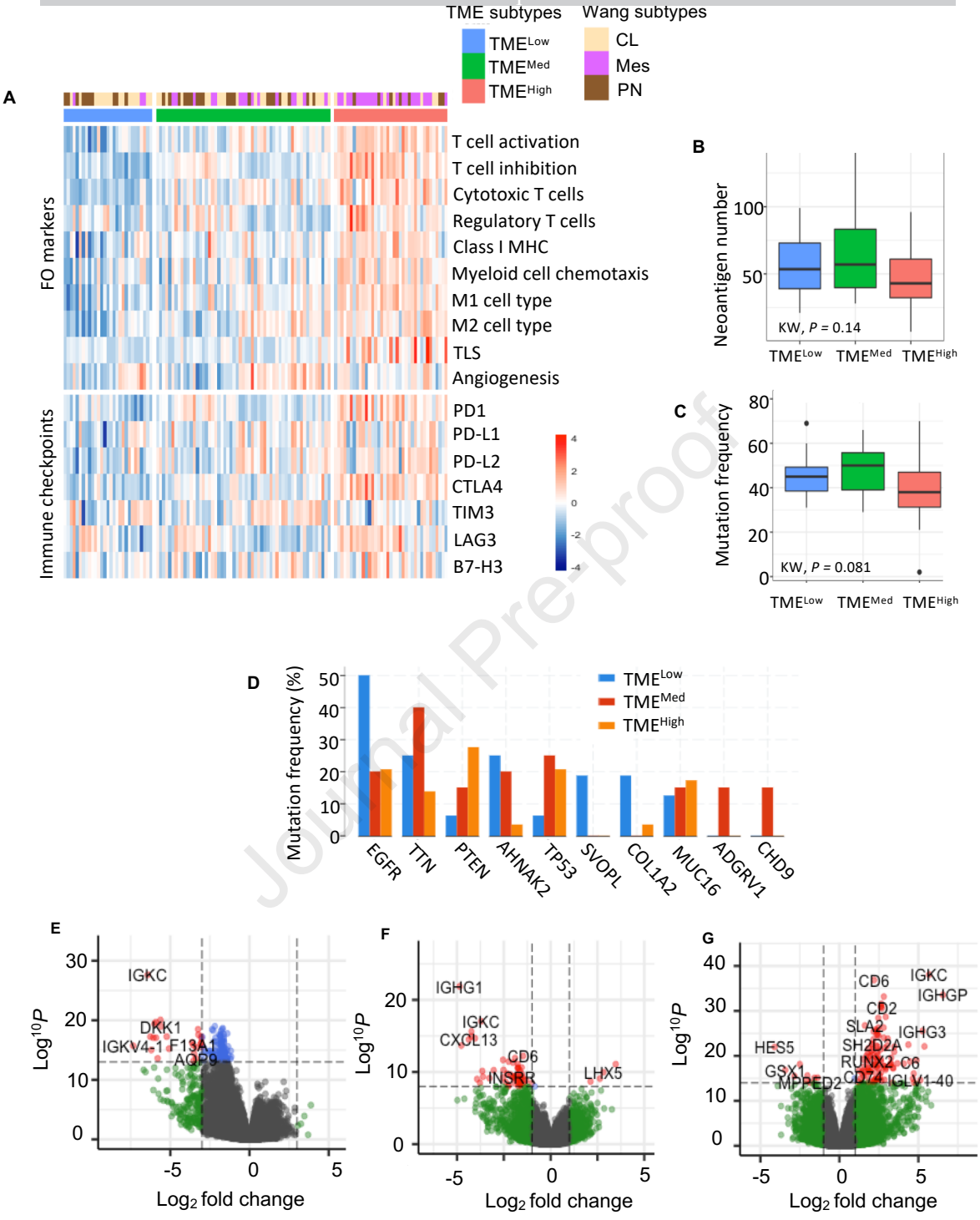

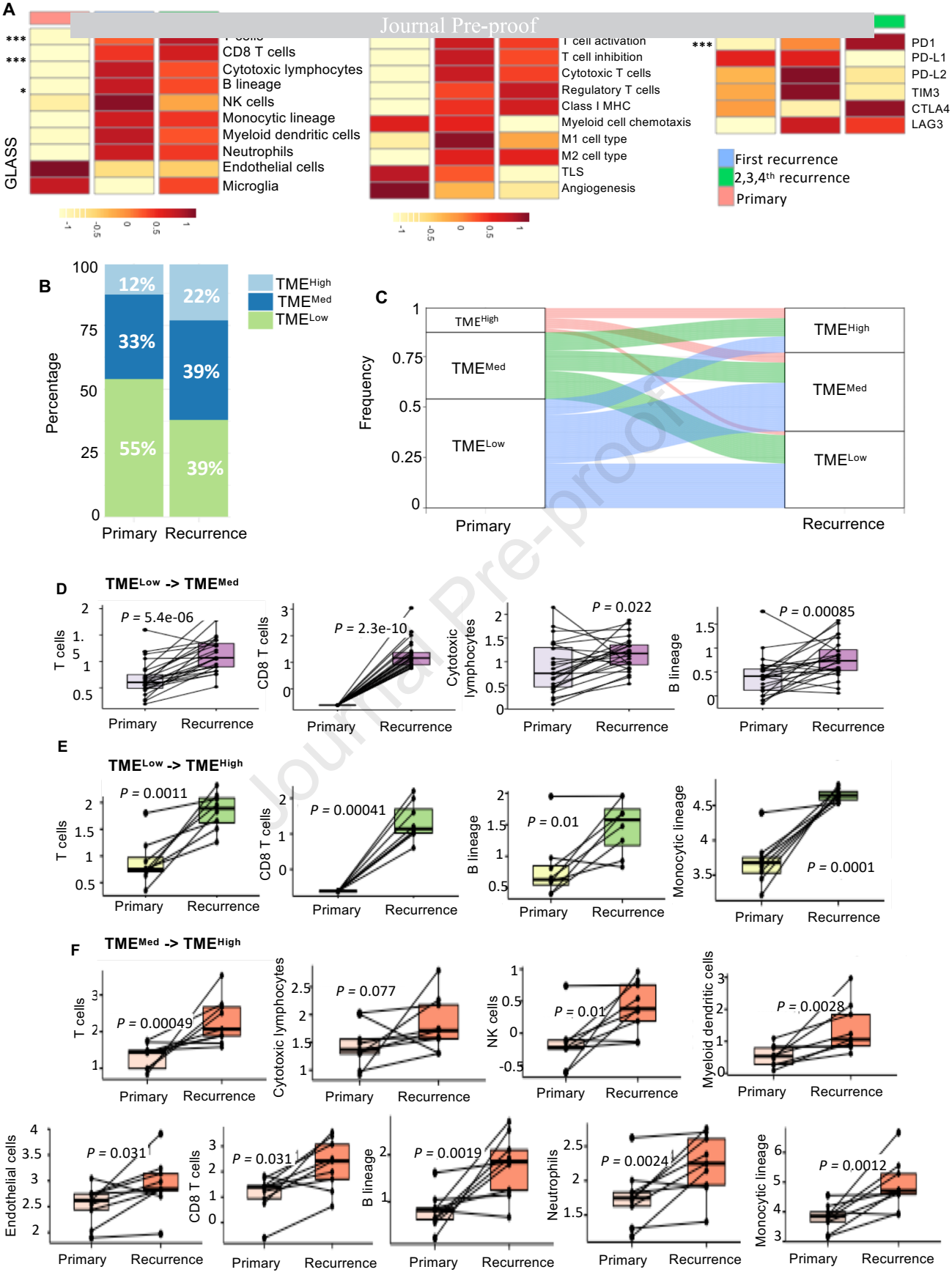

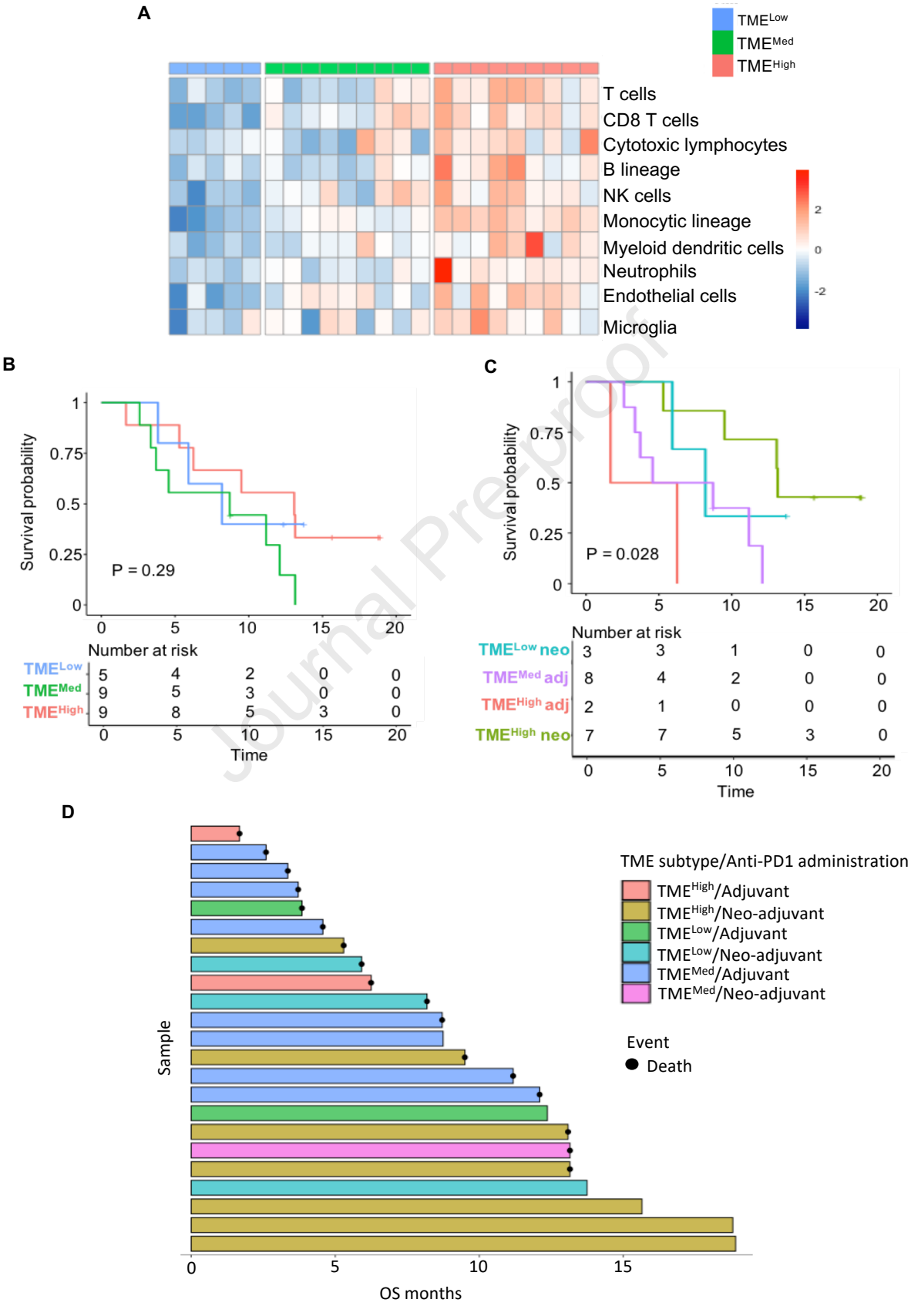
A
TME^Low
TME^Med
TME^High
T cells
CD8 T cells
Cytotoxic lymphocytes
B lineage
NK cells
Monocytic lineage
Myeloid dendritic cells
Neutrophils
Endothelial cells
Microglia
2
0
-2
B
Survival probability
P = 0.29
Number at risk
TME^Low 5 4 2 0 0
TME^Med 9 5 3 0 0
TME^High 9 8 5 3 0
Time
C
Survival probability
P = 0.028
Number at risk
TME^Low neo 3 3 1 0 0
TME^Med adj 8 4 2 0 0
TME^High adj 2 1 0 0 0
TME^High neo 7 7 5 3 0
Time
D
Sample
OS months
TME subtype/Anti-PD1 administration
TME^High/Adjuvant
TME^High/Neo-adjuvant
TME^Low/Adjuvant
TME^Low/Neo-adjuvant
TME^Med/Adjuvant
TME^Med/Neo-adjuvant
Event
Death